Hydrothermal scapolite related to the contact metamorphism of the Maladeta Plutonic Complex, Pyrenees: chemistry and genetic mechanisms

by Enrique Arranz[1], Marceliano Lago[1], Joaquín Bastida[2] and Carlos Galé[1]

Abstract

A detailed mineral composition study (EMP) of three different textural types of scapolite porphyroblasts in calc-silicate and microdiorite samples from the Maladeta Plutonic Complex (Central Pyrenees) is presented. Additionally, a scapolite mineral separate was characterised by XRD, TGA and IR spectrometry, in order to obtain reliable CO_2 and SO_3 estimates and crystallographic parameters. Many of the obtained compositions are Cl-rich and seem to be related, in their genesis, to the composition of the fluid phase. According to textural and chemical criteria, these scapolite porphyroblasts postdate the main contact metamorphism. The genesis of scapolite is interpreted as a result of the replacement of either metamorphic or igneous plagioclase, related to flow of NaCl- and $CaCO_3$-rich hydrothermal solutions around the intrusive complex. Other minerals (biotite) also seem to be involved in the replacement process affecting plagioclase in microdiorite. Reaction schemes are proposed for the genesis of scapolite in the different compositional groups considered in this paper. The growth of scapolite porphyroblasts was followed by the precipitation of hydrothermal scapolite as vein fillings, in optical and chemical continuity with previous crystals.

Keywords: scapolite, hydrothermal, mineral composition, contact metamorphism.

Introduction

The scapolite group, with the general formula $M_4T_{12}O_{24}A$ (M: Ca, Na, K, minor amounts of other cations; T: Si, Al; A: anionic groups, mainly, Cl^-, F^-, CO_3^{2-}, SO_4^{2-}) constitutes a solid-solution series between the ideal end-members marialite (Ma; $Na_4Al_3Si_9O_{24}Cl$) and meionite (Me; $Ca_4Al_6Si_6O_{24}CO_3$). Some authors (e.g. ORVILLE, 1975; AITKEN, 1983) also consider mizzonite (Me_{75}; $Ca_3NaAl_5Si_7O_{24}CO_3$) as the pure carbonate end-member and dipyre ($Na_3CaAl_4Si_8O_{24}Cl$) as the pure chlorine, carbonate-free end member (LIEFTINK et al., 1993), but these probably represent the effect of changes in substitutional mechanism rather than end-members (as proposed by AITKEN et al., 1984: HASSAN and BUSECK, 1988) and must be considered as varietal names (BAYLISS, 1987). TEERSTRA et al. (1999) described silvialite ($Ca_4Al_6Si_6O_{24}SO_4$) as the pure calcic-sulfate member, approved by the CNMMN of the International Mineralogical Association.

Scapolite occurrences have been described in many different geological environments (see SHAW, 1960a for a review), including regional metamorphic rocks (e.g. marbles and calc-silicate rocks, WHITE, 1959; amphibolite facies calcareous gneisses, SHAW, 1960b) and veins, granulitic xenoliths in basaltic and kimberlitic rocks (LOVERING and WHITE, 1964; DAWSON, 1971; STOLZ, 1987), igneous rocks (GOFF et al., 1982), and contact metamorphic rocks (e.g. calc-silicates, KERRICK et al., 1973) in some cases related to the hydrothermal effects induced by the intrusion of plutonic masses (CRISS et al., 1984) or deformation events (GOERGEN et al., 1999; KULLERUD and ERAMBERT, 1999).

Scapolite has also been described as a typical mineral of the low-pressure Upper Cretaceous metamorphism in the Pyrenees (RAVIER, 1959; RAVIER and THIEBAUT, 1982; GOLBERG et al., 1986; MONTIGNY et al., 1986; GOLBERG and LEYRELOUP, 1990) north of the Pyrenean Axial Zone. In a different geological context, scapolite was cited as part of the mineral assemblages in

---

[1] Depto. de Ciencias de la Tierra, Universidad de Zaragoza. C/Pedro Cerbuna, 12, E-50009 Zaragoza, Spain. <earranz@posta.unizar.es>

[2] Depto. de Geología, Universidad de Valencia (Estudi general). Burjassot. E-46100 Valencia, Spain.

contact metamorphic marbles and calc-silicates all around the Maladeta Plutonic Complex (MPC): CHARLET (1977, 1979), DELGADO (1993; this author provided electron microprobe analyses of this mineral, together with stable and radiogenic isotopic data on scapolite-bearing rocks) and ARRANZ (1997) described the occurrence of scapolite porphyroblasts from several locations within the contact aureole of the MPC. GARCÍA-BELLES (1998) described scapolite in porphyritic microdiorite dykes, emplaced within scapolite-bearing rocks of the contact aureole of the MPC. These dykes intruded previously metamorphosed country rocks as these dykes crosscut porphyritic granodiorite dykes, coeval to the main intrusive event of the Maladeta Massif (ARRANZ, 1997; GARCÍA-BELLES, 1998).

The origin of scapolite in many parts of the contact aureole of the MPC has been linked to the hypothetical presence of evaporite levels interbedded within the Devonian limestones (DELGADO, 1993). A close relationship between evaporite-derived fluids and the formation of scapolite has been proposed by several authors (KWAK, 1977; MOINE et al., 1981; VANKO and BISHOP, 1982; OWEN and GREENOUGH, 1999) but this genetic hypothesis must be supported, in any case, by direct observation of evaporite formations (or their relics) in the regional geological framework.

Previous models of scapolite formation in calc-silicate rocks (OTERDOOM and GUNTER, 1983; MOECHER and ESSENE, 1990; REBBERT and RICE, 1997) considered a relatively simple mechanism, which only implies plagioclase and calcite as reacting phases. KERRICK et al. (1973) proposed a more complete expression of the scapolite-forming reaction which included a NaCl-bearing fluid phase, stressing the role of fluids in the genesis of natural CO_3-Cl-scapolite occurrences:

$$3X \text{ anorthite} + 3Y \text{ albite} + X \text{ calcite} + (NaCl)_{fluid} = Me_xMa_y \qquad (2)$$
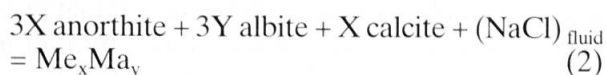
which is a suitable expression of the scapolite forming reaction stoichiometry. Several authors (SHAW, 1960b; OTERDOOM and GUNTER, 1983; MORA and VALLEY, 1989; MARKL and PIAZOLO, 1998; KULLERUD and ERAMBERT, 1999; ORVILLE, 1975; ELLIS, 1978; HUCKENHOLZ and SEIBERL, 1989) have evidenced that, in either natural and experimental plagioclase–scapolite assemblages, the Me/Ma ratio is not directly dependent of the An/Ab ratio of the coexisting plagioclase, and so the composition of the equilibrium fluid phase is the main control on the distribution coefficient for the scapolite forming reaction.

In this paper, we present a detailed study (electron microprobe, XRD, infrared spectroscopy and TGA) of the composition of scapolite crystals in three different types of contact metamorphic rocks and dykes from the Maladeta aureole, which allow us to propose a mainly hydrothermal origin for this mineral. These data, together with the textural and compositional features of coexisting mineral phases in the scapolite-bearing rocks, allow us to constrain the scapolite-forming processes, which in some cases are far more complex than considered in the previously cited models.

Geological context

The Maladeta Plutonic Complex (MPC; ARRANZ, 1997) is one of the biggest late Hercynian intrusive bodies outcropping within the Pyrenean Axial Zone (PAZ; Fig. 1A), with an outcrop area of more than 400 km². The complex is divided into two main units and several minor blocks by ductile shear bands, which also affect the host rocks (Fig. 1B). Both units of the MPC are made up of a similar intrusive sequence of basic rocks, granodiorites and two-mica syenogranites as the main rock types. Intrusion of the igneous complex took place into epizonal greenschist-facies metasediments, which were affected by contact metamorphism, resulting in the development of a contact aureole that, in some sectors, reaches over 1000 metres in thickness. The inner parts of the aureole were metamorphosed to pyroxene-hornfels facies, expressed by wollastonite or even periclase (now retrograded to brucite pseudomorphs) in calc-silicate rocks and sillimanite + alkali feldspar in pelitic rocks.

The studied area (Fig. 1C) is located in the inner part of the contact aureole of the western unit (the Aneto Unit; CHARLET, 1977; ARRANZ, 1997). The estimated P–T conditions of the contact metamorphism are 625 ± 25 °C and 2.5 kbar, according to mineral assemblages (Sil + Kfs in metapelites, periclase in dolomitic marbles; ARRANZ, 1997; Spl + Sil in metapelites; DELGADO, 1993), and cation exchange geothermometry (Grt–Bt, Grt–Ilm; DELGADO, 1993). This confirms the epizonal emplacement of the MPC. Host rocks in the studied area are the Silurian black shales, which crop out only as a narrow band in the core of an anticline, and the Lower Devonian series, composed of the typical sequence of formations defined by MEY (1967a,b) for the Sierra Negra Facies (Rueda, Basibé, Fonchanina and Mañanet formations). Considered as a whole, the host rocks include a variety of shales, arenites and limestones, and no evidence of evaporite interbeddings or their relics has been described in this part of the central Pyr-
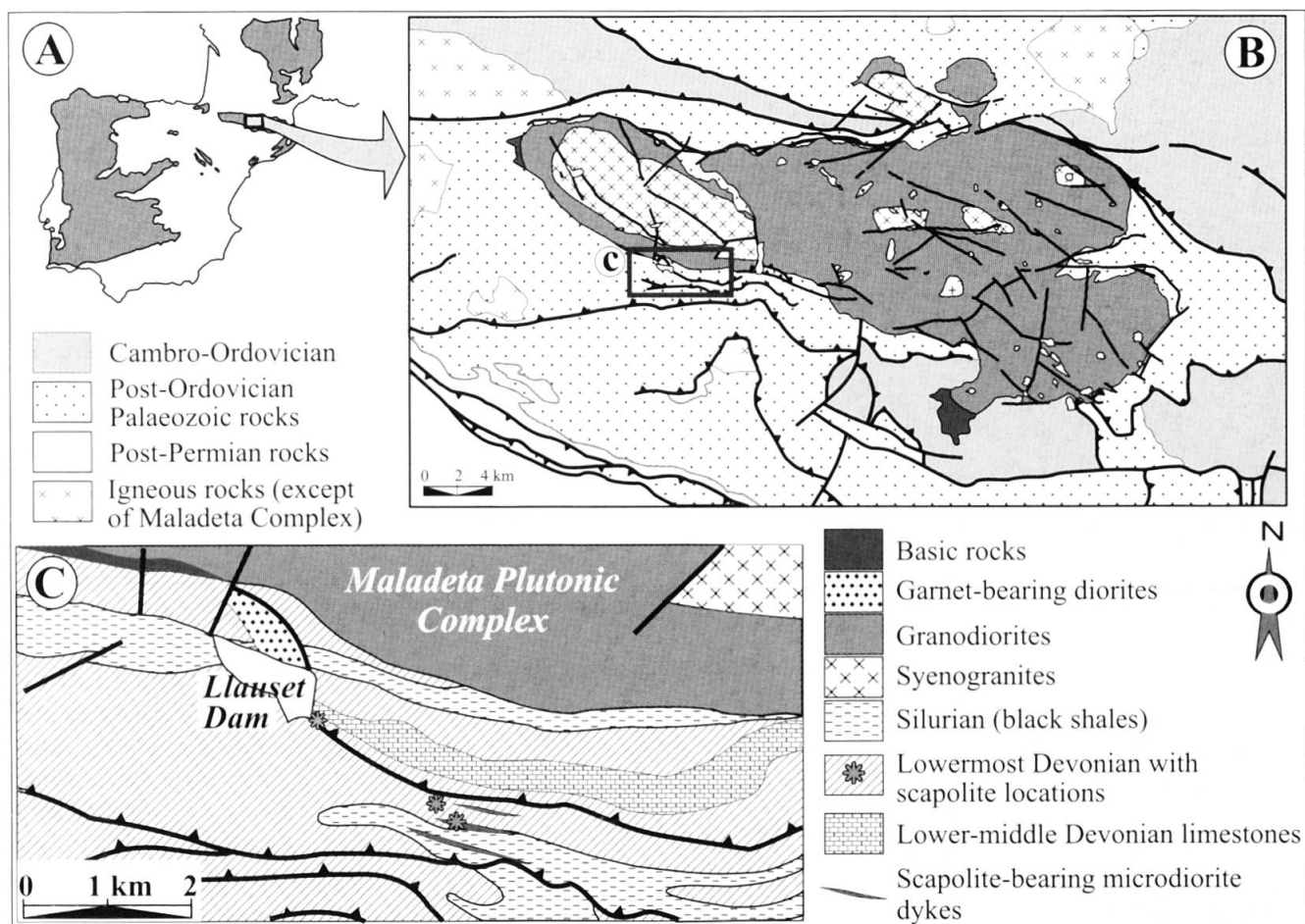
Fig. 1 Geological map of the studied area. (A) location of area (detailed in B in the context of the south-European Hercynian outcrops. (B) Geological sketch map of the Palaeozoic rocks of the Central Pyrenees and location of Fig. 1C. After POBLET (1991) and ARRANZ (1997). (C) Detailed map of the studied area of the Maladeta contact aureole and location of scapolite-rich rocks.

enees (MEY, 1967a,b; GARCÍA-SANSEGUNDO, 1992; GARCÍA-BELLES, 1998).

Scapolite crystals are widespread in the contact metamorphic aureole but are usually only observable under the microscope. In this sector of the aureole scapolite porphyroblasts, ranging in size from less than 1 mm up to 3 cm are quite common. These developed in the Devonian impure limestones and marls representing the Rueda and Basibé Formations (lowermost Devonian). These porphyroblasts are easily recognizable as they stand out on weathered surfaces.

Intrusion of the plutonic complex was dated at 295 ± 11 Ma (K/Ar in contact metamorphic phlogopite, SOLÉ et al., 1997) and was accompanied by injection of a variety of apical sills and dykes into the aureole (MEY, 1967b; GARCÍA-BELLES, 1998). One of these, an aplitic dyke, was dated at 298 ± 2.4 Ma (U/Pb in zircon; EVANS, 1993). Some of the sills (microdiorites) emplaced in scapolite-bearing rocks also contain scapolite. Locations of scapolite, in both metamorphic and igneous rocks, are given in Fig. 1C.

Sample description

The studied samples comprise the variety of scapolite-bearing rock types in the area and can be grouped into four different subsets:

I: A first group is composed of metamorphosed impure limestones containing scapolite porphyroblasts. Rocks of this type appear as massive or thick-bedded medium grained marbles, with a primary assemblage of calcite, phlogopite, talc, calcic amphibole and lesser amounts of plagioclase, tourmaline, quartz and titanite. Scapolite porphyroblasts (Fig. 2) are idioblastic and show reduced optical zoning. Inclusion trails (of any of the aforementioned minerals), inside these porphyroblasts demonstrate their post-kinematic character with respect to the main deformational event during contact metamorphism, whereas the previously indicated assemblage is probably syn-kinematic. This temporal ordering, together with the textural relationships between the primary assemblage and the scapolite porphyroblasts suggest that scapolite formed as a late phase, proba-
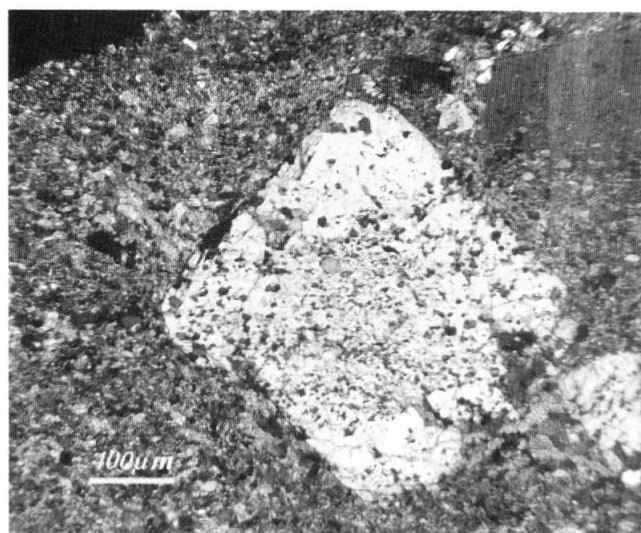
Fig. 2 Photomicrograph of type-I scapolite porphyroblasts. Note inclusion trails in the inner part of the crystal.

bly related to post-metamorphic hydrothermal flow. Fluid flow also lead to the precipitation of quartz and calcite in veins that crosscut the rock, connecting areas with scapolite porphyroblasts. Of the included minerals, phlogopite, calcite and plagioclase are less abundant inside the scapolite crystals when compared with the bulk rock.

II: A second subset is represented by a mineral concentrate extracted from a type-I sample. Extraction of the scapolite crystals was made by washing the sample in 1N hydrochloric acid, in order to dissolve calcite impurities. Individual scapolite crystals were hand-picked from the insoluble residue. The scapolite content of this concentrate is more than 99.5%, the only impurities being tiny inclusions (mostly quartz, phlogopite, titanite and calcite) inside the crystals, unextractable by acid rinse. These inclusions were determined under the microscope on single grain mounts. SWAYZE and CLARK (1990) found that this separation method has no detectable influence on the structurally bonded CO_3^{2-}, HCO_3^-, or HSO_4^- anionic groups.

III: Samples of calc-silicate rocks, with scapolite poikiloblasts. These samples are representative of the most widespread scapolite-bearing rocks in the studied part of the aureole, covering from the innermost aureole to several hundreds of metres away from the contact. The primary assemblages of these calc-silicates are variable, from diopside + wollastonite + vesuvianite + plagioclase + opaque minerals + titanite ± alkali feldspar close to the contact, to calcic amphibole + diopside + plagioclase + phlogopite + opaque minerals + titanite ± alkali feldspar ± calcite in more

external areas. In these latter rocks, clinozoisite, actinolite and chlorite occur as late minerals, overprinting the primary assemblage and frequently as vein fillings. In all of the samples of this group, scapolite occurs as xenoblastic poikiloblasts (clinozoisite, titanite, diopside and alkali feldspar are the main inclusion phases), up to 2 cm in size, dispersed in the rock. Many of these crystals are related to small discontinuities in the rock (microfractures), which are infilled by scapolite (in optical continuity with scapolite in the rock, Fig. 3) and other minerals (mainly quartz and calcite but also actinolite). Optically, these scapolite poikiloblasts show irregular zoning.

IV: Microdiorite samples: microdiorite dykes (related to the intrusion of the Maladeta Massif) outcropping far from the contact show a primary mineral assemblage composed of plagioclase, biotite, quartz, subhedral titanite, calcic amphibole and opaque minerals (ilmenite and magnetite), but in the inner aureole, many of these dykes are emplaced within scapolite-bearing rocks, and this mineral is also part of the mineral assemblage. Anhedral scapolite crystals poikilitically enclose every other mineral of the primary assemblage. From a textural point of view, these scapolite crystals occupy intercrystalline spaces or, more commonly, replace plagioclase crystals, using mineral cleavage planes as the primary discontinuities (Fig. 4). In scapolite-rich samples scapolite crystals (up to 45 vol%) enclose tiny ilmenite and magnetite grains that are commonly associated with xenoblastic microgranular titanite. Biotite, which is abundant in the rock is rare inside the scapolite, pointing to a complex replacement process that generated scapolite crystals in these samples. Calcic amphibole is also common in the microdiorite and inside scapolite crystals, although its modal abundance is slightly reduced inside the scapolite. Zoning in these scapolite crystals is strongly irregular (see below), perhaps because several crystals of plagioclase (and other minerals) may have been replaced by a single scapolite crystal.

Scapolite crystals in these four groups of samples share some common features: (a) scapolite is always a late phase that includes or replaces primary igneous or metamorphic mineral phases; (b) reduced optical zoning, with an irregular pattern in most of the crystals, and (c) many of the scapolite crystals are related to veins and discontinuities in the rocks. As pointed out before, these features support a post-metamorphic and mainly hydrothermal origin for this mineral in the studied rocks.
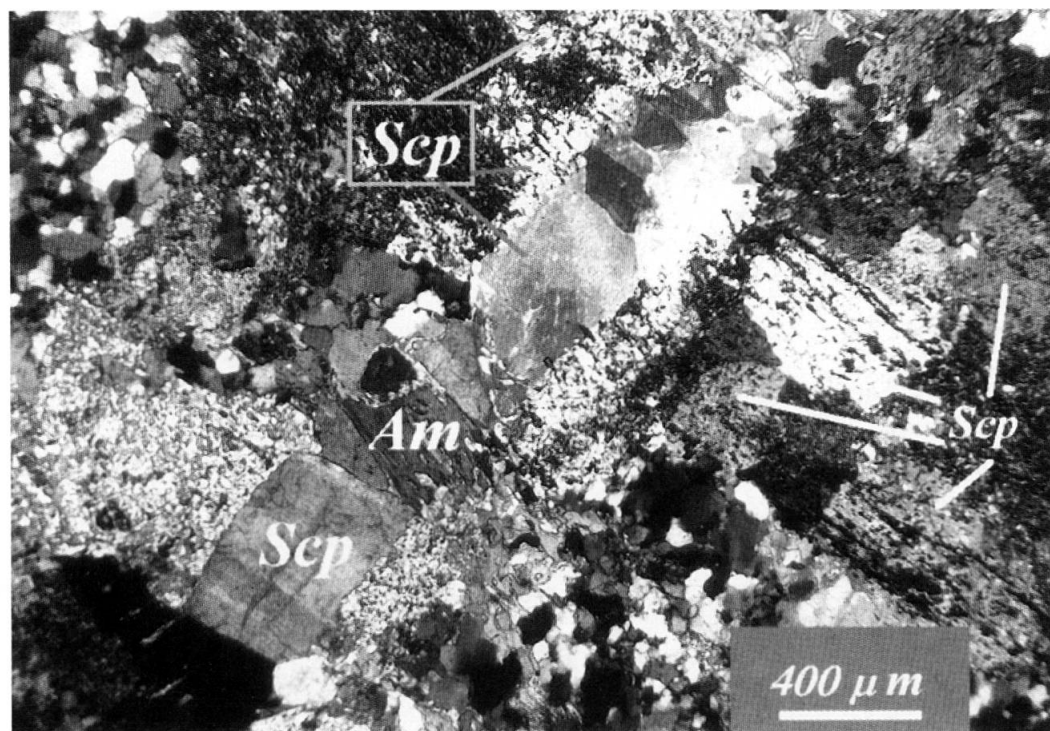
Fig. 3 Photomicrograph of a type-III sample, injected by a hydrothermally (scapolite + amphibole) filled vein; scapolite poikiloblasts in contact with the vein are in optical continuity with those inside the vein.
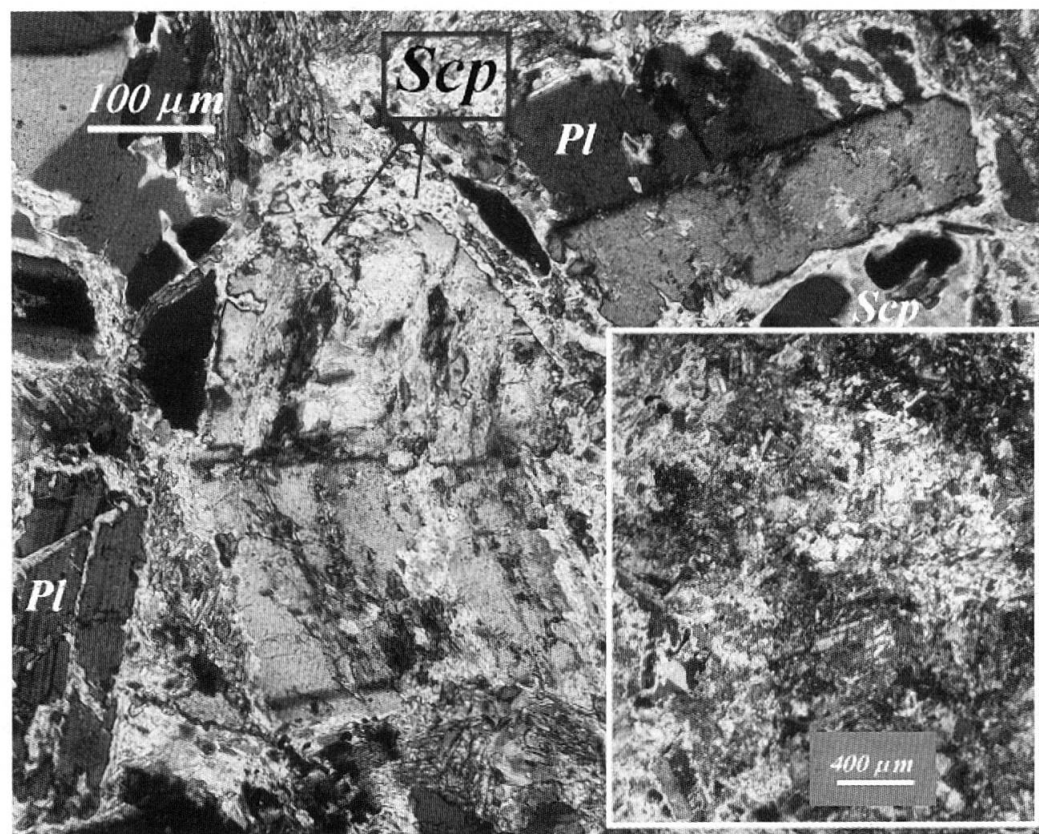

Fig. 4 Photomicrograph of a type-IV sample, showing replacement of plagioclase by scapolite poikiloblasts. Whitish areas in the general view (rectangle in the lower-right corner) show the size and irregular shape of these scapolite poikiloblasts.

Table 1   X-ray diffraction data of scapolite powder. Remarks: Ov – overlapping; Q hkl – quartz reflection; C hkl – calcite reflection; Nr – number of the overlapping peak.

Nr	hkl	$(2\theta)_{ob}$	$(2\theta)_{cal}$	$\Delta(2\theta)$	d_{cal}	Ir	Remark
1	110	10.282	10.300	0.018	8.5815	3.2	
2	101	13.774	13.752	-0.022	6.4343	1.6	
3	200	14.579	14.586	0.007	6.0681	14.3	
4	211	20.095	20.098	0.003	4.4145	3.9	
5	220		20.684		4.2908	9.5	ov Q 100
6	310	23.175	23.158	-0.017	3.8378	35.7	
7	002		23.427		3.7943		ov 6 Nr 6
8	301	24.912	24.923	0.011	3.5698	10.9	
9	112	25.650	25.650	0.000	3.4702	100	
10	202	27.740	27.707		3.2171	1.5	
11	321	29.024	28.997	-0.027	3.0769	86.3	
12	400		29.415		3.0340		
13	330		31.244		2.8605	5.4	
14	222		31.448		2.8424	5.7	
15	411	32.590	32.604	0.014	2.7442	14.0	
16	420		32.981		2.7137	13.2	
17	312	33.191	33.176	-0.015	2.6982	43.7	
18	103		36.247		2.4763	2.6	
19	510	37.770	37.767		2.3801	<2.6	
20	402		37.940		2.3696	2.6	
21	431		38.926		2.3118	(13.5)	broad
22	213	39.253	39.263		2.2927	<1	
23	332	39.443	39.418		2.2841	10.9	
24	422		40.850		2.2073	3.1	
25	521		41.778		2.1604		broad
26	440		42.084		2.1454	11	
27	303		42.097		2.1448		ov Q 200
28	530	43.497	43.444	-0.053	2.0813	3.2	
29	600		44.770		2.0227		ov Nr 30
30	323		44.783		2.0222		ov Nr 31
31	512	44.891	44.921	0.03	2.0162	10.5	
32	611	47.072	47.057		1.9296	9.1	ov C 024
33	620	47.383	47.335		1.9189	24.9	
34	413	47.398	47.347		1.9184		
35	004	48.002	47.912	-0.09	1.8971	13.7	
36	442		48.720		1.8675	<1	
37	114		49.144		1.8524	<2.3	
38	541	49.556	49.531	-0.025	1.8389	3.8	
39	532		49.938		1.8248	6.4	
40	204		50.354		1.8107	12.6	ov C 310
41	602		51.134		1.7849	<1	
42	631		51.916		1.7598	5.2	broad
43	503	52.261	52.186	-0.075	1.7514	4.1	
44	224		52.712		1.7351	<1	
45	550		53.335		1.7163	5.8	
46	622		53.468		1.7124	9.9	
47	314		53.864		1.7007	<1	
48	701		54.226		1.6902	<1	
49	640		54.478		1.6830		ov Nr 50
50	523	54.509	54.488	-0.021	1.6827	4.1	
51	721		56.471		1.6282	4.1	broad
52	404		57.224		1.6086	4.2	ov Q 210
53	730		57.814		1.5935	<1	
54	334		58.315		1.5810	<1	
55	613		58.908		1.5665	5.3	
56	712	59.009	59.022	0.013	1.5638	8.9	ov Nr 56
57	424		59.394		1.5549	<1	
58	642		60.093		1.5384	3.3	ov Q 311
59	651		60.798		1.5223		<1
60	800		61.031		1.5170	<1	
61	543	61.109	61.041	-0.068	1.5168	8.2	ov Nr 61
62	105		61.527		1.5060		<1

Table 2 Representative EMP scapolite analyses and structural formulae for the different textural types considered in this paper. Me% was calculated as $100\times(\Sigma$divalent cations)/4 according to TEERSTRA and SHERRIFF (1997); EqAn was calculated as (Al-3)/3 (ORVILLE, 1975). The detection limits (calculated as 3 times the standard deviation of the background count; REED, 1993) for minor elements are:Ti: 0.06%; Cr: 0.08%; Ni:0.07%; Fe:0.14; Mn: 0.11; MgO: 0.03; Ba: 0.1%; Sr: 0.09%; F: 0.22%; Cl: 0.21%. n.a: not analysed. b.d – below the detection limit. (1) includes Mn=0.02, (2) includes Ba=0.02 and Sr=0.05, (3) includes Mg=0.01 and Fe^{2+}=0.02, (4) includes Fe^{2+}=0.02.

| Type | I-II | I-II | I-II | I-II | III | III | III | III | III | IV | IV | IV | IV | IV | IV | IV | IV |
| Sample | CL-4 | CL-4 | CL-4 | CL-4 | 325A | 325A | 325 | 325 | 325 | JGB-61 | JGB-61 | JGB-61 | JGB-61 | JGB-27 | JGB-27 | JGB-27 | JGB-27 |
Analysis	14	15	17	4	25	27	34	36	38	40	50	52	66	2	8	9	19
SiO₂	49.70	49.59	49.68	49.16	50.61	50.84	49.18	48.93	49.86	50.73	48.99	50.56	49.53	49.39	50.33	49.54	50.42
TiO₂	0.07	b.d	0.07	b.d	0.23	0.07	b.d	b.d	0.09	b.d	b.d	b.d	b.d	b.d	b.d	b.d	b.d
Al₂O₃	25.08	25.21	25.44	25.48	25.53	25.27	25.29	25.39	24.61	24.93	25.43	24.43	25.58	25.22	23.96	25.73	25.53
Cr₂O₃	b.d	b.d	b.d	b.d	b.d	0.72	b.d	b.d	b.d	0.08	0.13	0.00	b.d	0.11	b.d	b.d	b.d
NiO	b.d	b.d	b.d	b.d	0.28	0.08	b.d	b.d	0.09	0.18	b.d	b.d	b.d	b.d	0.08	b.d	b.d
FeO	b.d	b.d	b.d	b.d	b.d	b.d	b.d	b.d	b.d	b.d	b.d	0.17	b.d	b.d	b.d	b.d	0.16
MnO	b.d	b.d	b.d	b.d	b.d	0.18	b.d	b.d	b.d	b.d	b.d	b.d	b.d	b.d	b.d	b.d	b.d
MgO	b.d	b.d	b.d	b.d	b.d	b.d	b.d	b.d	b.d	b.d	b.d	0.03	b.d	b.d	b.d	b.d	b.d
CaO	14.52	14.32	14.37	14.65	15.59	14.86	14.13	14.96	12.87	12.55	13.48	11.31	14.53	14.11	11.65	14.62	13.95
Na₂O	5.34	5.47	5.56	5.33	4.92	5.20	5.51	4.84	6.08	6.36	5.90	6.51	5.19	5.39	6.58	5.32	5.75
K₂O	0.83	0.92	0.89	0.94	0.49	0.60	0.80	0.65	0.77	0.69	0.62	0.80	0.68	0.37	0.57	0.38	0.37
BaO	n.a	n.a	n.a	n.a	0.42	b.d	b.d	b.d	b.d	b.d	b.d	b.d	b.d	b.d	b.d	b.d	b.d
SrO	n.a	n.a	n.a	n.a	0.58	b.d	b.d	b.d	b.d	b.d	b.d	b.d	b.d	b.d	b.d	b.d	b.d
F	b.d	b.d	b.d	b.d	b.d	b.d	b.d	b.d	b.d	b.d	b.d	b.d	b.d	b.d	b.d	b.d	b.d
Cl	1.67	1.85	1.77	2.00	1.14	1.30	1.58	1.33	1.88	2.00	1.81	2.35	1.57	1.46	2.18	1.42	1.52
Total(-O=F,Cl)	96.83	96.94	97.37	97.11	99.54	98.80	96.14	95.80	95.82	97.07	95.96	95.64	96.72	95.72	94.86	96.68	97.36
Structural formulae on the basis of 16 total cations																	
Si	7.48	7.46	7.43	7.39	7.47	7.52	7.44	7.45	7.56	7.59	7.41	7.68	7.46	7.51	7.70	7.46	7.53
Al	4.45	4.47	4.48	4.52	4.44	4.40	4.51	4.56	4.40	4.39	4.54	4.38	4.54	4.52	4.32	4.56	4.49
Sum (T)	11.93	11.92	11.91	11.91	11.90	11.92	11.94	12.00	11.95	11.98	11.95	12.06	12.01	12.03	12.02	12.02	12.02
Ti	0.01	–	0.01	–	0.03	0.01	–	–	0.01	–	–	–	–	–	–	–	–
Cr	–	–	–	–	–	0.08	–	–	–	0.01	0.02	0.00	–	0.01	–	–	–
Ni	–	–	–	–	0.03	0.01	–	–	0.01	0.02	–	–	–	–	0.01	–	–
Na	1.56	1.59	1.61	1.55	1.41	1.49	1.61	1.43	1.79	1.85	1.73	1.92	1.52	1.59	1.95	1.55	1.66
Ca	2.34	2.31	2.30	2.36	2.46	2.35	2.29	2.44	2.09	2.01	2.18	1.84	2.35	2.30	1.91	2.36	2.23
K	0.16	0.18	0.17	0.18	0.09	0.11	0.15	0.13	0.15	0.13	0.12	0.16	0.13	0.07	0.11	0.07	0.07
Sum (M)	4.07	4.08	4.09	4.09	4.10	4.08	4.06	4.00	4.05	4.02	4.05	3.94	3.99	3.97	3.98	3.98	3.98
Cl	0.43	0.47	0.45	0.51	0.29	0.32	0.41	0.34	0.48	0.51	0.46	0.60	0.40	0.38	0.56	0.36	0.38
%Me	57.76	56.58	56.46	57.65	62.44	59.77	56.41	61.08	52.05	50.44	54.13	47.41	58.75	58.04	48.07	59.23	56.48
EqAn	0.48	0.49	0.49	0.51	0.48	0.47	0.50	0.52	0.47	0.46	0.51	0.46	0.51	0.51	0.44	0.52	0.50
					(2)	(1)						(3)					(4)

Analytical methods

Powder X-ray diffraction (XRD) was used for mineralogical identification and crystallographic characterisation of scapolites in all the samples. XRD patterns were obtained at the University of Valencia from samples powdered to less than 50 µm in grain size, using a D500 Siemens diffractometer (operating at 40 kV, 30 mA; Ni filtered Cu Kα; step scanning: 0.02°, 3 sec./step; range: 2–62°, 2θ). The programs EVA and MAINT of the Diffrac-Plus package (Bruker AX systems) were used for evaluation of X-ray powder data and identification.

Scapolite crystals were analysed in samples belonging to subtypes I, III and IV using a CAMECA SX-50 electron microprobe (EMP) at the University of Oviedo, operating in WDS mode at 15 kV accelerating potential, 15 nA beam current, 3 µm beam diameter and 10 seconds of counting time for all the elements except Na, F and Cl. The counting time for F and Cl was set at 20 s, keeping the rest of the analytical conditions

unchanged. The analytical conditions for Na were 20 µm beam diameter, 15 kV accelerating potential, 10 nA beam current and 10 s of counting time. Under these conditions, the reproducibility of the analytical values for Na was proven to be better than ±0.2 wt% by iteration of analysis on the same spot. All the results were corrected for interelemental effects by a ZAF-procedure. The standards used were orthoclase (K, Si), wollastonite (Ca), albite (Na, Al), pyrophanite (Mn, Ti), hematite (Fe), strontianite (Sr), barite (Ba), apatite (F), vanadinite (Cl) and synthetic MgO, Cr_2O_3, Rb_2O and NiO. The same analytical conditions were used for analysis of plagioclase, biotite and amphibole in type-IV scapolite-bearing microdiorites.

The mineral separate (type II) was also studied by infrared absorption spectrophotometry (IR) and thermogravimetric analysis (TGA) at the University of Valencia. The IR spectrum was obtained on a pressed disc of the powdered sample dispersed in KBr, using a Nicolet 410 FTIR spectrometer equipped with a DTGS (deuterated

Table 3 Representative EMP analyses and structural formulae for plagioclase crystals in microdiorite dykes. Abbreviations and detection limits as in Table 2.

Sample *Analysis*	JGB-27 1	JGB-27 3	JGB-27 6	JGB-27 8	JGB-27 10	JGB-61 18	JGB-61 20	JGB-61 21	JGB-61 22	JGB-61 23
SiO_2	48.36	47.84	45.41	48.40	48.82	49.81	50.72	47.27	51.19	53.38
Al_2O_3	32.29	32.07	33.39	31.39	31.59	31.18	30.57	32.73	30.39	28.43
MgO	b.d	0.12	0.07	0.09	0.11	b.d	b.d	0.14	0.02	b.d
CaO	15.75	15.93	17.36	15.41	15.45	15.10	14.29	16.67	13.97	12.40
FeO	0.32	0.44	0.36	0.56	0.55	0.44	0.52	0.61	0.43	0.33
SrO	b.d	0.10	0.13	b.d	0.10	b.d	0.13	b.d	b.d	b.d
BaO	b.d	b.d	b.d	b.d	b.d	b.d	0.12	b.d	b.d	0.10
Na_2O	2.51	2.59	1.75	2.61	2.73	2.98	3.46	1.92	3.80	4.67
K_2O	b.d	b.d	b.d	b.d	b.d	0.09	0.09	0.12	0.10	0.13
Rb_2O	b.d	b.d	b.d	0.13	0.12	0.14	0.09	0.08	0.13	0.08
Total:	99.24	99.07	98.46	98.59	99.47	99.74	99.88	99.55	100.04	99.42

Structural formulae on the basis of 8 oxygens

Si	2.231	2.218	2.129	2.251	2.252	2.286	2.321	2.186	2.337	2.437
Al_{IV}	1.756	1.752	1.845	1.721	1.718	1.687	1.649	1.784	1.635	1.530
Sum (T)	3.987	3.971	3.974	3.972	3.970	3.973	3.970	3.971	3.971	3.966
Mg	–	0.008	0.005	0.007	0.007	–	–	0.010	0.002	–
Ca	0.779	0.791	0.872	0.768	0.763	0.743	0.701	0.826	0.683	0.606
Fe	0.012	0.017	0.014	0.022	0.021	0.017	0.020	0.024	0.017	0.012
Sr	–	0.003	0.003	–	0.003	–	0.003	–	–	–
Na	0.225	0.232	0.159	0.235	0.244	0.265	0.307	0.172	0.336	0.413
K	–	–	–	–	–	0.005	0.005	0.007	0.006	0.007
Rb	–	–	–	0.004	0.003	0.004	0.003	0.002	0.004	0.002
Total:	5.00	5.02	5.03	5.01	5.01	5.01	5.01	5.01	5.02	5.01
An:	77.6	77.3	84.6	76.5	75.8	73.3	69.2	82.2	66.6	59.0
Ab:	22.4	22.7	15.4	23.5	24.2	26.2	30.3	17.2	32.8	40.2
Or:	0.0	0.0	0.0	0.0	0.0	0.5	0.5	0.7	0.6	0.7

Table 4 Representative EMP analyses and structural formulae for amphibole crystals in microdiorite dykes. 13eCNK – normalisation to 13 cations except Ca, Na and K. Abbreviations and detection limits as in Table 2.

Sample	JGB-27	JGB-27	JGB-27	JGB-27	JGB-27
Analysis	3	4	5	6	10
SiO_2	51.07	51.01	51.55	51.04	50.03
TiO_2	0.20	0.20	0.32	0.27	0.51
Al_2O_3	5.25	4.51	4.96	4.84	5.83
Cr_2O_3	0.09	b.d	b.d	b.d	0.09
FeO(tot)	13.66	13.23	13.44	13.36	13.56
MgO	13.57	14.14	13.78	14.00	13.35
MnO	0.21	0.20	0.30	0.33	0.44
CaO	12.82	12.70	12.54	12.84	12.55
Na_2O	0.33	0.35	0.44	0.43	0.44
K_2O	0.17	0.16	0.17	0.17	0.24
Total	97.46	96.76	97.67	97.41	97.13

Structural formulae on the basis of 13eCNK cations

Si	7.47	7.50	7.52	7.46	7.36
Al_{IV}	0.53	0.50	0.48	0.54	0.64
Sum T:	8.0	8.0	8.0	8.0	8.0
Al_{VI}	0.37	0.29	0.38	0.30	0.38
Ti	0.02	0.02	0.03	0.03	0.06
Cr	0.01	–	–	–	0.01
Fe^{3+}	0.0	0.0	0.0	0.0	0.0
Mg_C	2.96	3.10	3.00	3.05	2.93
Fe^{2+}_C	1.63	1.59	1.59	1.62	1.63
Sum C:	5.0	5.0	5.0	5.0	5.0
Fe^{2+}_B	0.04	0.04	0.05	0.01	0.04
Mn_B	0.03	0.03	0.04	0.04	0.06
Ca	2.01	2.00	1.96	2.01	1.98
Na_B	0.00	0.00	0.00	0.00	0.06
Sum B:	2.07	2.06	2.05	2.06	2.14
Na_A	0.047	0.051	0.062	0.060	0.000
K	0.016	0.015	0.016	0.016	0.022
Sum A:	0.06	0.07	0.08	0.08	0.02
Total cations	15.13	15.13	15.13	15.14	15.16
mg*	0.64	0.66	0.65	0.65	0.64
Class.	Mg-Hbl	Act	Act	Mg-Hbl	Mg-Hbl

triglycine sulphate) detector, over the range of 4000 to 400 cm^{-1} wavenumbers; 16 scans were accumulated, all performed at a resolution of 4 cm^{-1}.

TGA was carried out using a Universal V2.4F (TA Instruments) system, adjusted at 50 °C, configured to obtain a ramp of 5.00 °C/min. up to 500 °C and 10.00 °C/min. from 500 to 1300 °C. The N_2 flux was fixed at 104 ml/min.

Results

The refined and indexed lattice spacings (in agreement with the *I4/m* group) for the scapolite mineral concentrate (type-II), as calculated by means of the program by GARVEY (1990) are given in Table 1. Lattice parameters computed by the Win-Metric program (Bruker AX Systems) are: a = b = 12.014 (±0.036)Å; c = 7.607 (±0.011)Å.

Meionite contents were computed from diffraction data on the same samples as analysed by EMP, by the procedure of BURLEY et al. (1964) using the spacings obtained. A nearly constant value of 61% Me was calculated for all of the samples, which is close to the compositions obtained by EMP analysis (see below) for type-III and also with the Me-rich values for type-I–II samples.

Representative EMP analyses and structural formulae of scapolite crystals are given in Table 2. A 16-cation basis was chosen for normalisation, as this scheme minimises the effect of analytical errors for Si and Al and leads to more realistic values for the M cations (MORA and VALLEY, 1989). Analyses with Si + Al outside of the 12 ± 0.1 atoms per formula unit (a.p.f.u) interval were discarded from the original set of 115 EMP analyses. The obtained compositions are quite pure, and only minor amounts of K in the M-site are significant. The rest of the analysed minor elements, in-

Table 5 Representative EMP analyses and structural formulae for biotite crystals in microdiorite dykes. Normalisation of analyses according to the scheme of LAIRD and ALBEE (1981): cations per 11 oxygens and Σ cations–Ca–Na–K = 7. Abbreviations and detection limits as in Table 2.

Sample	JGB-26	JGB-26	JGB-26	JGB-26	JGB-26
Analysis	3	7	11	13	16
SiO_2	36.84	36.63	36.82	36.23	37.40
TiO_2	2.20	1.71	1.76	1.85	1.75
Al_2O_3	16.04	16.25	16.84	15.84	16.60
MgO	11.87	11.44	11.65	11.55	12.35
CaO	0.11	b.d	0.09	b.d	b.d
MnO	0.18	0.29	0.15	0.19	0.12
FeO	17.68	19.04	18.23	18.09	16.69
K_2O	9.27	9.68	9.61	9.93	9.71
Cl	0.32	0.44	0.24	0.43	0.34
Total	94.69	95.48	95.38	94.10	94.96
(–O = Cl)	0.07	0.10	0.05	0.10	0.08
Total*	94.62	95.38	95.33	94.00	94.88

Cations per 11 oxygens (Σcats – CNK = 7)

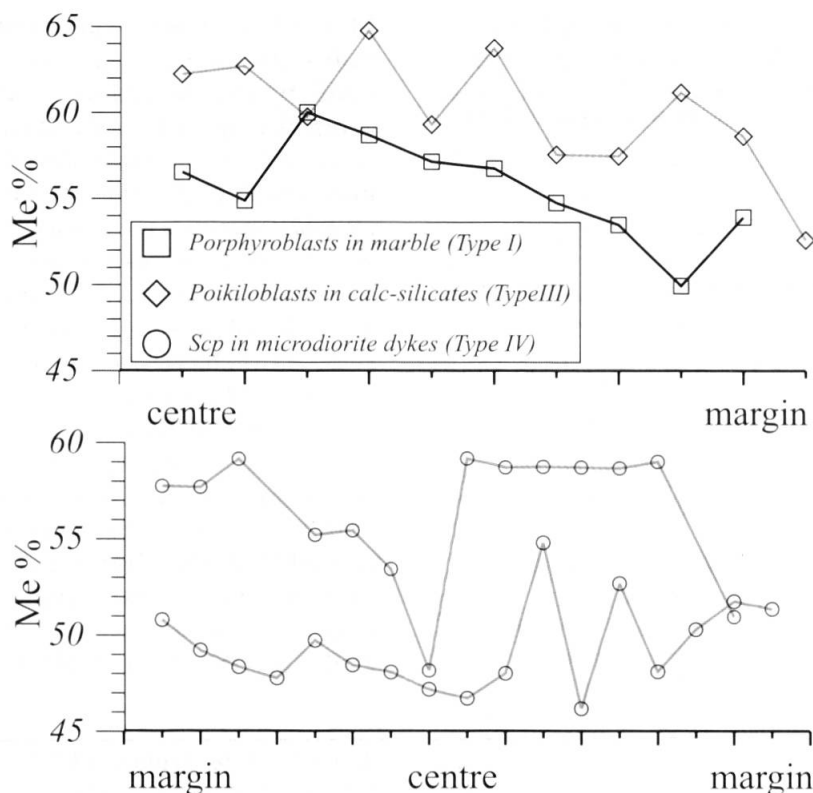|					
Si	2.80	2.79	2.79	2.80	2.82
Al IV	1.20	1.21	1.21	1.20	1.18
Sum T:	4.00	4.00	4.00	4.00	4.00
Al VI	0.24	0.25	0.29	0.24	0.30
Ti	0.13	0.10	0.10	0.11	0.10
Mg	1.35	1.30	1.31	1.33	1.39
Ca	0.01	–	0.01	–	–
Mn	0.01	0.02	0.01	0.01	0.01
Fe^{2+}	1.13	1.21	1.15	1.17	1.05
Sum M	2.86	2.88	2.88	2.86	2.85
K	0.90	0.94	0.93	0.98	0.94
Cl	0.04	0.06	0.03	0.06	0.04
Total	7.81	7.88	7.84	7.89	7.83
fe*	0.46	0.48	0.47	0.47	0.43

Fig. 5 Compositional profiles for scapolite in type-I and type-III samples (upper graph) and for type-IV samples (lower graph). Spacing of analytical points not to scale.
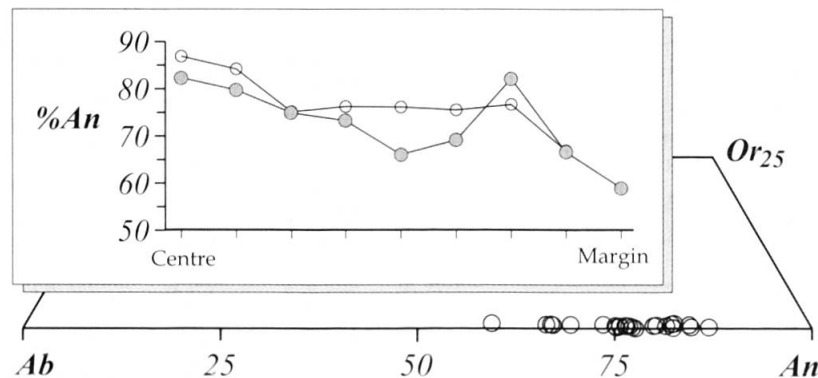

Fig. 6 Composition and profiles for plagioclase crystals in type-IV samples (microdiorites). Spacing of analytical points not to scale.

cluding F, are below the detection limits for most of the analyses. Representative EMP analyses for plagioclase crystals in microdiorites, including type-IV scapolite crystals, are given in Table 3. Representative compositions for amphibole and biotite crystals in microdiorites are given in Tables 4 and 5 respectively.

Meionite contents (calculated as $100 \times \Sigma[\text{di-valent cations}]/4$, as proposed by TEERSTRA and SHERRIFF, 1997) range from 64.7 to 46.7 Me%, the highest values corresponding to type-III samples (Me% 64.7–52.6; average Me: 61.4%) and type I-II (Me%: 61.2–53.1; average Me: 58.2%). Type-IV samples are less meionitic on average (Me: 55%), although displaying a wider variation range

(46.7–59.2 Me%). Despite these ranges in Me% for each sample type, it is worth noting that each single crystal shows a limited variation range in Me%, which is always less than 10% for type I–II samples and less than 15% for types III and IV. These features are visible in single-crystal Me% profiles (Fig. 5), which correspond to the optical zoning features observed under the microscope. Profiles across scapolite crystals of types I and III display a decrease in Me% from the centre to the rim, with oscillations in type-III and a more continuous variation in type-I scapolite. Profiles of type-IV scapolites reveal irregular zoning, probably reflecting the composition of pre-existing plagioclase crystals, as some of the zoning patterns
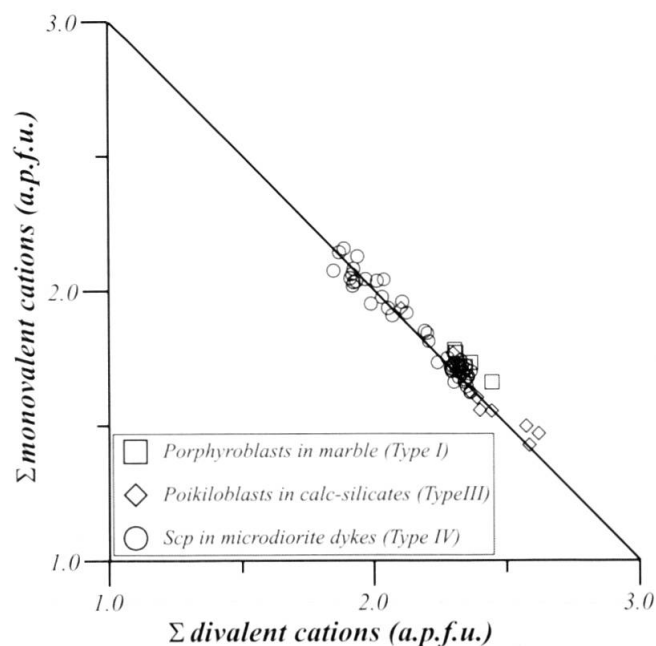
Fig. 7 Σ monovalent cations vs. Σ divalent cations diagram for scapolite compositions presented in this study.

are similar to features observed in plagioclase profiles (Fig. 6). Figure 7 indicates stoichiometric sums and a 1:1 substitution of monovalent and divalent cations in the M site as the main mechanism of compositional variation.

According to CHAMBERLAIN et al., (1985), electrostatic energy calculations suggest that Na^+ and Ca^{2+} atoms tend to be ordered, respectively, around Cl^- and CO_3^{2-} in the structure of scapolite, composing Na_4Cl and $Ca_4(CO_3)$ clusters. This ordering minimises the electrostatic energy of the structure, and local charge balance in the anion site is achieved. Changes in this configuration related to the substitution $NaCl (CaCO_3)_{-1}$ lead to an increase in the energy of the structure as local charge imbalances appear in anion sites when the configuration of the cation-anion clusters is changed. These local charge imbalances do not affect the electrical neutrality of the whole crystal. Thus, for any given $Al/(Si + Al)$ ratio there is a unique $Ca/(Ca + Na)$ ratio for which local charge balance in the anion site exists; any other $Ca/(Ca + Na)$ value (between the limits imposed by the stoichiometry of this mineral) implies charge imbalances in the A-site. For example, the substitution of $NaCl$ by $CaCO_3$ in a Na_4Cl cluster yields a relative excess of negative charges in the A-site and, therefore, the CO_3^{2-} anion is electrically underbonded as it is surrounded by one Ca and three Na atoms.

In a $Ca/(Ca + Na)$ vs. $Al/(Si + Al)$ plot (Fig. 8), showing the contours of local charge balance calculated by CHAMBERLAIN et al., (1985), all the analyses presented in this paper lie above the

local charge balance line, in the field of carbonate-rich members and express a relative excess of negative charges in the A site. This is common in carbonate members of the scapolite group (CHAMBERLAIN et al., 1985), as a result of the substitution of $NaCl$ by $CaCO_3$.

Structural formulae, as expressed in Table 2, allow the calculation of the excess positive charge (EPC) p.f.u., following the indications of TEERSTRA and SHERRIFF (1997): EPC = Σ monovalent cations + $2\times\Sigma$ divalent cations) – $(Al^{3+} + Fe^{3+})^{IV}$. A plot of Cl contents (measured by EMP) vs. EPC (Fig. 9) shows that the EPC values for most of the analyses are considerably higher than explained by the $Cl-CO_3^{2-}$ substitution. This difference can be related to the $NaCl(CaCO_3)_{-1}$ substitution mechanism, which is able to yield compositions with high values of EPC as Ca enters in the structure replacing Na and also, an excess of CO_3^{2-} in the A-site. On the other hand, all of the analysed crystals display low to moderate chlorine contents (0.28–0.60 a.p.f.u.), even those crystals occurring in pure calc-silicates (types I and III). The Cl-rich analyses presented here are in agreement with those of the less calcic Cl-scapolite presented by KULLERUD and ERAMBERT (1999).

Estimation of other anions present in the A-site was made indirectly by means of IR spectroscopy and TGA. Both kinds of analyses were carried out on the type-II mineral concentrate. The IR absorbance spectrum obtained (Fig. 10) shows the characteristic peaks for C–O and H–O···H bonds (SCHWARCZ and SPEELMAN, 1965; SWAYZE and CLARK, 1990) and also less defined absorbance peaks in the wavenumbers interval 3540–3640, which can be assigned either to the hydroxyl stretches from OH groups in the A-site or to protonated structural oxygen atoms (SWAYZE and CLARK, 1990). According to these authors, some small peaks around 3500 wavenumbers can be assigned to hydroxyl stretches of HCO_3^- and HSO_4^- (Fig. 10). Most of the vibrational frequencies of S-bearing oxy-anions are, unfortunately, obscured by framework or C–O vibrational frequencies. The CO_2 and SO_3 contents (2.4 and 0.88 wt% respectively) were derived from IR data, through the range of 1007 to 1425 wavenumbers, according to the method of SCHWARCZ and SPEELMAN (1965) and the empirical relationship between CO_2 and SO_3 found by these authors for scapolite crystals already presented by SHAW (1960b).

The TGA curve obtained on the mineral separate (type-II) shows a nearly continuous weight loss from 50 °C up to 1200 °C (Fig. 11), and is quite similar to those obtained by GRAZIANI and LUCCHESI (1982). The curve can be divided into six sections, defined by changes in the slope: 50–230
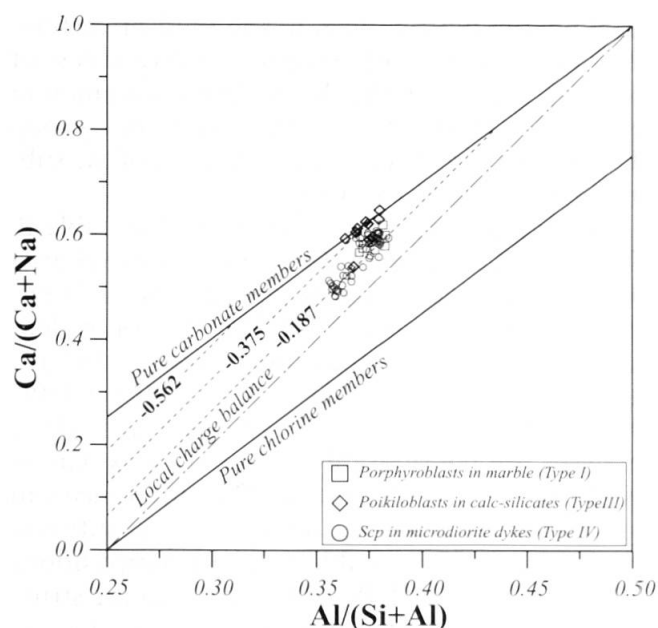
Fig. 8 Ca/(Ca + Na) vs. Al/(Si + Al) diagram of the analysed scapolites. Local charge balance contours (after CHAMBERLAIN et al., 1985) show a slight excess of negative charges in the A-site.
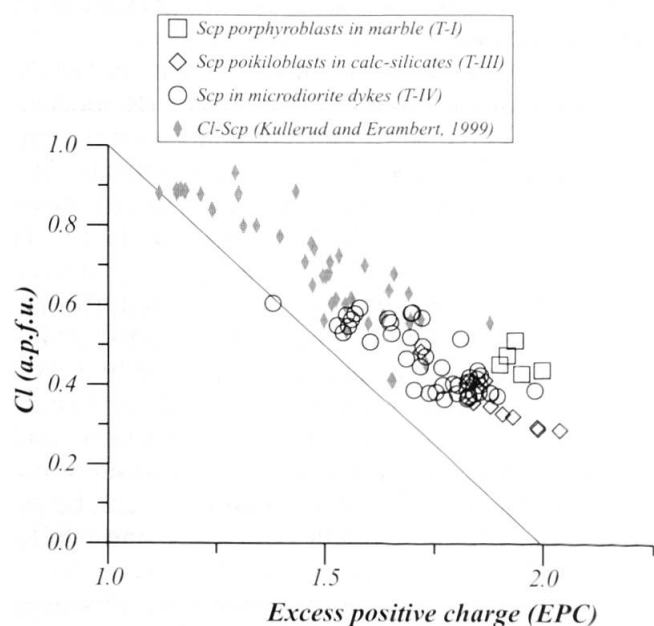

Fig. 9 Chlorine a.p.f.u. vs. Excess Positive Charge plot (EPC; calculation according to TEERSTRA and SHERRIFF, 1997; see text.). Published data for Cl-scapolite (KULLERUD and ERAMBERT, 1999) have been included, showing a coherent compositional trend, away from the simple Cl–CO₃ substitution line.

°C, 230–560 °C, 560–605 °C, 605–830 °C, 830–1050 °C and finally, 1050–1210 °C. According to GRAZIANI and LUCCHESI (1982), the 3.86% weight loss observed for the 830–1210 °C interval should be assigned to NaCl and KCl volatilization and the weight losses below 830 °C (1.3%) could

be correlated to H_2O, CO_2 and SO_2 releases. Calculation of maximum KCl + NaCl releases using the Cl, Na_2O and K_2O analytical data obtained by EMP for scapolite crystals in a type-I sample yields values in the range 2.9–3.7 wt%, which are consistent with the TGA data. These results also suggest that part (0.1 to 0.9 %) of the weight loss measured over 830 °C could also correspond to CO_2 and SO_2, in agreement with their estimated contents from the IR data.

Calculation of the anions p.f.u. for a "model" Me_{61} scapolite, according to diffraction data, considering the CO_2 (2.4%) and SO_3 (0.88%) estimates, yields C = 0.496 a.p.f.u. and S = 0.101 a.p.f.u., with an average Cl content of 0.43 a.p.f.u. The resulting occupancy of the A-site for this composition is 1.03 atoms (C + S + Cl) which fits well with the ideal formula. According to this ideal composition, no significant amount of H_2O is necessary to fill the A-site, but this component may be present, event in small amounts (0.5 wt% H_2O, as a maximum; SHAW, 1960b; EVANS et al., 1969) as indicated by many authors (e.g. SCHWARCZ and SPEELMAN, 1965; GRAZIANI and LUCCHESI, 1982; TEERSTRA and SHERRIFF, 1996, 1997) and also suggested by our IR data.

Assuming that both C and S build complex divalent species (CO_3^{2-}, SO_4^{2-}, SO_3^{2-}; SCHWARCZ and SPEELMAN, 1965; GRAZIANI and LUCHESSI, 1982; TEERSTRA and SHERRIFF, 1997), the total negative charge of analysed and estimated anions in the A-site would be close to 1.65, which is clearly lower than the calculated EPC (close to 1.9) for these scapolite crystals. This difference is probably related to the uncertainties in CO_2 and SO_3 contents determined by the empirical method of SCHWARCZ and SPEELMAN (1965).

Compositional relationships between the different scapolite types show a linear trend, when plotted in binary variation diagrams that involve Cl. As the composition of the three groups of scapolite-bearing rocks considered in this paper is clearly different, this common behaviour suggests that an external compositional factor, related to the fluid phase is the link between the different scapolite types. A Cl vs. Ca/(Ca + Na) plot (Fig. 12) is especially instructive, comparing the scapolite compositions considered in this work with those obtained by DELGADO (1993) for similar scapolite-bearing calc-silicate rocks from the same area, and published data (SHAW, 1960a; DEER et al., 1963; GRAZIANI and LUCCHESI, 1982; TEERSTRA and SHERRIFF, 1997; KULLERUD and ERAMBERT, 1999). All the analyses presented in this paper fit the same general trend, which is almost parallel to that defined by the KULLERUD and ERAMBERT (1999) data set. In both groups of
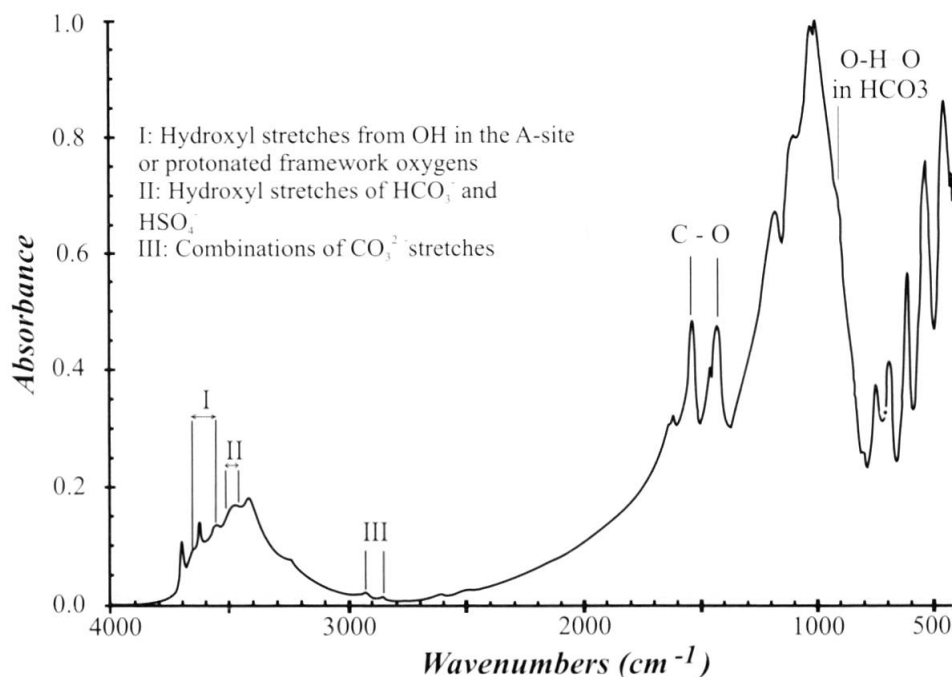
Fig. 10   IR absorbance spectrum of the scapolite mineral separate (type-II).

samples, the less calcic compositions yield the most Cl-rich values. This is clearly seen for type-I and some type-IV samples, which are notably more Cl-rich for a given Ca value, when compared to the rest of the data, even those representing Cl-rich scapolites.

Discussion: origin of the fluid phase and genetic mechanisms

Scapolite analyses presented here, even pertaining to different textural types, are compositionally related, and belong to the carbonate-rich members of the solid solution series, as expected for the composition of the scapolite-bearing calc-silicate rocks and also of the most common host-rock of the dykes containing type-IV scapolite.

Some of the analysed crystals display Cl-rich compositions, which are not very common in scapolite crystallised in the presence of excess calcite (ORVILLE, 1975). This suggests that this mineral formed under a relatively high activity of Cl in the fluid phase. TEERSTRA and SHERRIFF (1997) and PAN et al. (1994) indicate that Cl contents in scapolite are mainly controlled by charge-balance constraints imposed by the framework, and the activity of Cl in the equilibrium fluid phase influences only the modal abundance of scapolite, as Cl increases the stability of this mineral. These statements differ from conclusions of JIANG et al. (1994), who stated that the NaCl activity of the coexisting equilibrium fluid is the main controlling factor for the Cl contents of scapolite. If we

accept that the composition of the scapolite is controlled by the a_{CaCO3}/a_{NaCl} ratio in the fluid phase, as clearly stated by ORVILLE (1975), then high a_{NaCl} values in the fluid phase must be expressed in a relatively Na- and Cl-rich scapolite (ELLIS, 1978), even if we consider carbonate-hosted systems. Under these conditions, the composition of scapolite probably represents the maximum Cl contents – according to stoichiometric and charge-balance constraints – for the resulting framework, which is primarily controlled by the An contents in pre-existing plagioclase.

The origin of such a NaCl-rich fluid phase is probably related to a regional or local feature of the intrusive environment. As noted previously, no evidence for evaporite levels has been de-
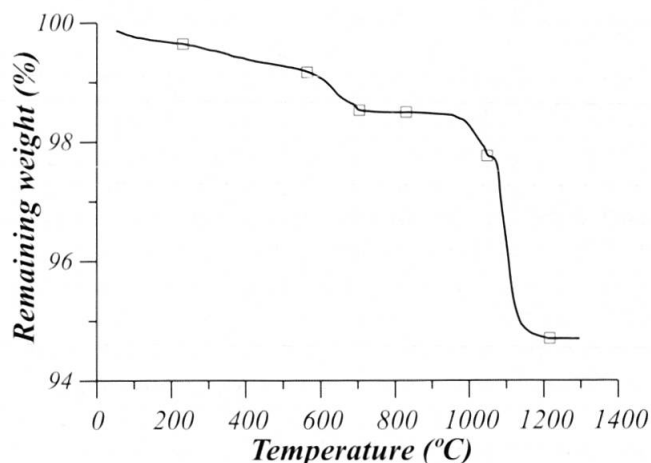

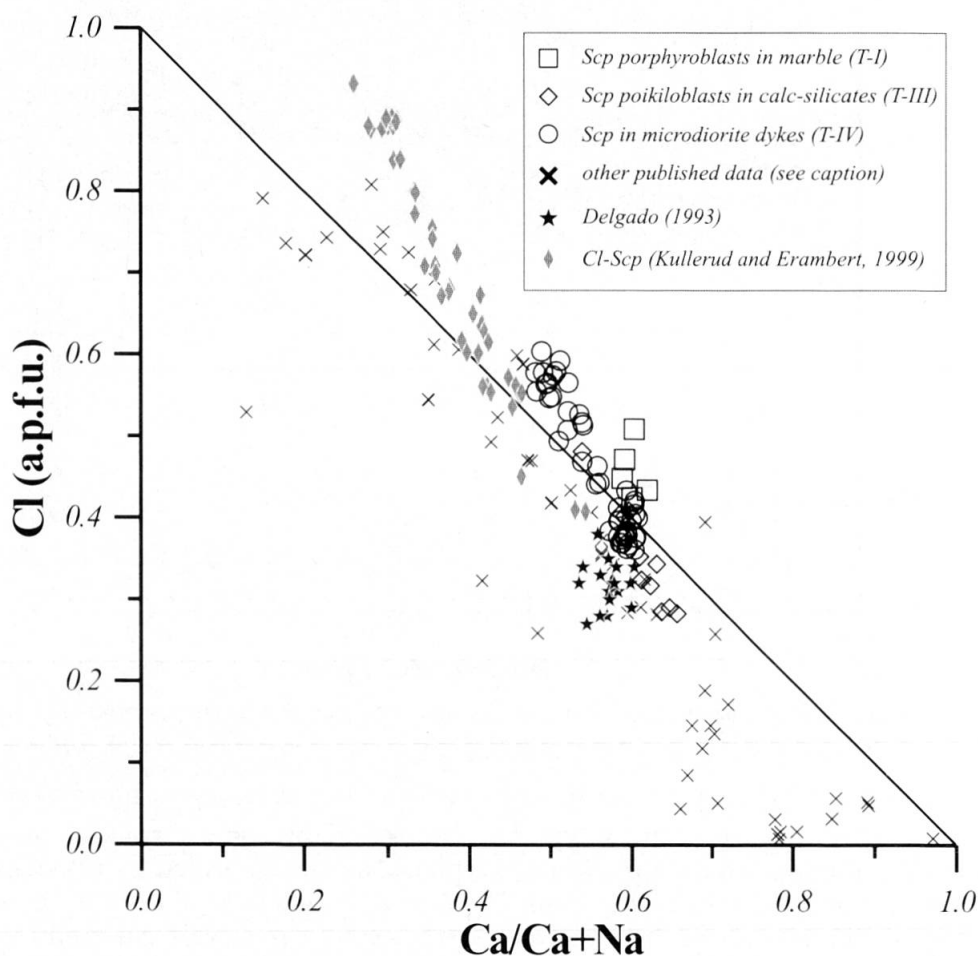*Fig. 11*   TGA curve for the scapolite mineral separate (type-II).

Fig. 12 Chlorine vs. Ca/(Ca + Na) plot for studied compositions compared with data presented in DELGADO (1993), KULLERUD and ERAMBERT (1999) and other previously published data (SHAW, 1960a; DEER et al., 1967; GRAZIANI and LUCCHESI, 1982; TEERSTRA and SHERRIFF, 1997). The compositions presented in this paper seem to be genetically related and are more Cl-rich than all the rest of compositions for a given Ca content.

scribed in the pre-Permian series of the Pyrenees (BARNOLAS and CHIRON, 1996) and, especially in the surroundings of the studied area, so an eva-porite-related origin for the fluid phase implied in the genesis of scapolite seems unlikely.

Several authors have proposed the development of large hydrothermal systems during Hercynian metamorphism in the Pyrenees (WICKHAM and OXBURGH, 1986; WICKHAM and TAYLOR, 1987; BICKLE et al., 1988), prior to anatectic melting and emplacement of late-Hercynian granitoid stocks. These hydrothermal systems imply the movement of surface waters (meteoric or even marine waters) through a thick section of upper crust (10–12 km; WICKHAM and OXBURGH, 1986). Intrusion of the granitoid masses in the Pyrenees took place at relatively shallow levels in the crust (6–8 km; DEBON et al., 1996) and, in consequence, promoted the installation of local hydrothermal systems, which mobilised both juvenile and crustal waters (probably similar to those proposed by WICKHAM and OXBURGH, 1986). Fluid inclusion
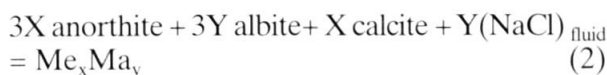
analysis of primary inclusions in three mineral-ised skarns developed at the northern contact of the Maladeta Complex (DELGADO, 1993), yields salinity values in the range 25–30% $NaCl_{eq}$ and homogenisation temperatures in the range 160–200 °C, which are in the normal compositional range for calc-silicate rocks (CRAWFORD et al., 1979a,b). These values are, nevertheless, mini-mum estimates, as DELGADO (1993) studied fluid inclusions in minerals (quartz, calcite) related to the late hydrothermal events of the skarn evolution. Similar salinity values were presented recently (GLEESON et al., 2000) for fluid inclusions in post-Hercynian mineralised veins around the Cornubian batholith (NaCl contents up to 25.9%, for inclusions with $NaCl_{eq} = 26.4\%$); these authors also provide data of $CaCl_2$ concentrations, which, in most of the cases, are within the range 3–8%. Taking all this data into account, scapolite crystal-lisation in the studied area could have taken place in presence of a NaCl-rich fluid phase, related to hydrothermal circulation of upper crustal waters

(with the minor addition of juvenile – i.e. granitic fluids).

The formation of scapolite in scapolite-plagioclase bearing calc-silicate rocks has traditionally been modelled (e.g. OTERDOOM and GUNTER, 1983; MOECHER and ESSENE, 1990; REBBERT and RICE, 1997) using the simplified phase reaction:
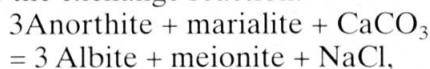
$$3 \text{ anorthite} + \text{calcite} = \text{meionite} \qquad (1)$$
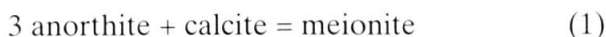
or, considering a more general expression (KERRICK et al., 1973)

$$3X \text{ anorthite} + 3Y \text{ albite} + X \text{ calcite} + Y(\text{NaCl})_{\text{fluid}} = \text{Me}_x\text{Ma}_y \qquad (2)$$

As previously stated, this component equation describes the stoichiometry of the scapolite-forming reaction. Several authors have dealt with the stability and phase relationships of plagioclase–calcite–scapolite assemblages; HUCKENHOLZ and SEIBERL (1989) showed experimentally that scapolite in the range 0.65–0.80 equivalent anorthite (EqAn = (Al–3)/3) may coexist with a plagioclase either rich in albite or in anorthite. These results are supported by the analyses of natural assemblages (OTERDOOM and GUNTER, 1983). The scapolite–plagioclase–calcite–NaCl system was studied, from an experimental point of view, by ORVILLE (1975). According to him, the relationship between the Ca/Na ratios of plagioclase and scapolite coexisting in equilibrium depends on the $a_{\text{CaCO3}}/a_{\text{NaCl}}$ ratio in the fluid phase and also on the An content of plagioclase, which are related by the expression:
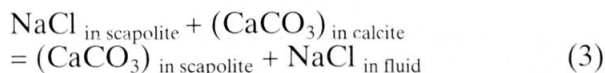
$$K_{T,P,An_x} = \frac{a_{Me}}{a_{Ma}} \frac{a_{NaCl}}{a_{CaCO_3}}$$

where K is related to the equilibrium constant for the exchange reaction:
3Anorthite + marialite + CaCO$_3$
= 3 Albite + meionite + NaCl,
once the composition of plagioclase has been fixed to a constant An$_x$ value.

ELLIS (1978) investigated experimentally at 750 °C and 4 kbar, the exchange reaction:

NaCl $_{\text{in scapolite}}$ + (CaCO$_3$) $_{\text{in calcite}}$
= (CaCO$_3$) $_{\text{in scapolite}}$ + NaCl $_{\text{in fluid}}$ $\qquad (3)$

For a scapolite of fixed EqAn content, the distribution coefficient for this reaction is:

$$K_D = \frac{(X_{CaCO_3}^{Scp})(X_{NaCl}^{fluid})}{(X_{NaCl}^{Scp})(X_{CaCO_3}^{calcite})} \qquad (4)$$

where X_i^j are the mole fractions of the i component in the respective phases (j). From measured values of K_D for reaction (3), Ellis (1978) derived the expression:

$$\ln K_D = -0.0028(X_{Al})^{-5.5580} \qquad (5)$$

where X_{Al} is the Al/(Si + Al) atomic ratio in scapolite. According to this expression, it is possible to estimate the X_{NaCl} (= NaCl/(NaCl + H$_2$O)) of the fluid phase coexisting with scapolite of a given composition at 750 °C and 4 kbar, at least to a first approximation, assuming that NaCl and CaCO$_3$ mix ideally in scapolite and NaCl and H$_2$O mix ideally in the fluid phase. MORA and VALLEY (1989) and OLIVER et al. (1992) discussed these assumptions, stressing the non-ideal behaviour of the NaCl–H$_2$O–CO$_2$ system at high concentrations of NaCl, as demonstrated by BOWERS and HELGESON (1983a,b), and so, corrections to the X_{NaCl} value should be made considering the influence of X_{CO2} in the fluid phase.

These experimental results are not directly applicable to the studied scapolite-bearing assemblages, as the experimental conditions differ substantially from the contact metamorphic-hydrothermal environment of the Maladeta aureole and also because those reactions involve either solid NaCl or CaCO$_3$ or both, which are not present in any of the studied rocks. Nevertheless, the relationships between the components in the solid and fluid phases, related by equilibrium constants or distribution coefficients are valid independently of the value of K for any particular P,T conditions. As a first approximation, X_{NaCl} values were calculated (using equations 4 and 5) for the fluid phase that coexisted with the studied scapolite crystals in calcite-bearing rocks (types I and III); the X_{NaCl} values for type-I scapolite are in the range 0.20–0.21, and a wider range (0.17–0.22) is obtained for analyses of type-III scapolite. If these values are interpreted in terms of NaCl-salinity of the fluid phase, they agree quite well with the fluid inclusion data furnished by DELGADO (1993). Nevertheless, these calculated values must be considered as a rough approximation to real values.
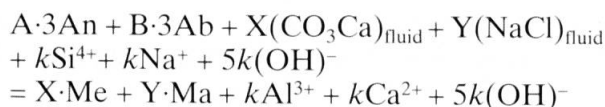
Any reaction scheme proposed to explain the formation of scapolite from plagioclase-bearing rocks in the presence of a NaCl–CaCO$_3$-bearing fluid phase, must take into account that the composition of the involved plagioclase and that of the fluid phase are not necessarily linearly dependent. According to ORVILLE (1975), the composition of the fluid phase is the main factor that controls the development of either more calcic or more sodic scapolite compared to the coexisting plagioclase. Additionally, the reaction scheme must consider that the fluid phase may change in composition as the reaction progresses and some elements may be added to the fluid phase as ionic or complex species.

If we take into account these constraints, we can write a first approximation to the 3·plagioclase + fluid = scapolite reaction scheme
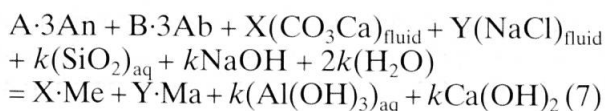
$$A·3An + B·3Ab + X(CO_3Ca)_{fluid} + Y(Na\,Cl)_{fluid} = X·Me + Y·Ma \quad (6)$$
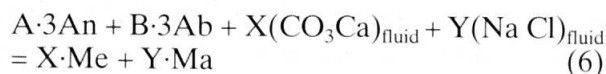
where $A = X_{An}$ in plagioclase, $B = X_{Ab}$ in plagioclase, $X = X_{Me}$ in scapolite and $Y = X_{Ma}$ in scapolite. This reaction is balanced only if $A = X$ and $B = Y$ (then, this reaction is equivalent to the scheme of KERRICK et al., 1973).
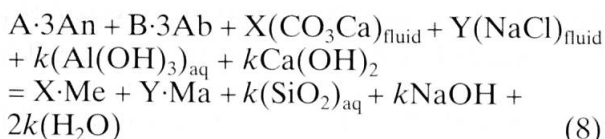
If $A/B > X/Y$, then the reaction is balanced considering:

$$A·3An + B·3Ab + X(CO_3Ca)_{fluid} + Y(NaCl)_{fluid} + kSi^{4+} + kNa^+ + 5k(OH)^- = X·Me + Y·Ma + kAl^{3+} + kCa^{2+} + 5k(OH)^-$$

where k equals the absolute value of $3(A–X)$. Little is known about the speciation of Si, Na, Al and Ca at high temperatures but, extrapolating the available data for lower temperatures, the suitable Si and Al aqueous (aq) species involved in this reaction could be $(SiO_2)_{aq}$ and $(Al(OH)_3)_{aq}$. If these species are considered, then the reaction is balanced according to the expression:
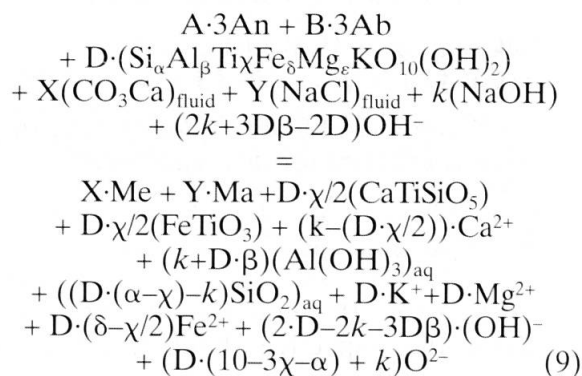
$$A·3An + B·3Ab + X(CO_3Ca)_{fluid} + Y(NaCl)_{fluid} + k(SiO_2)_{aq} + kNaOH + 2k(H_2O) = X·Me + Y·Ma + k(Al(OH)_3)_{aq} + kCa(OH)_2 \quad (7)$$

on the other hand, if $A/B < X/Y$:

$$A·3An + B·3Ab + X(CO_3Ca)_{fluid} + Y(NaCl)_{fluid} + k(Al(OH)_3)_{aq} + kCa(OH)_2 = X·Me + Y·Ma + k(SiO_2)_{aq} + kNaOH + 2k(H_2O) \quad (8)$$

The reaction scheme proposed in reaction (7) can be considered a reasonable approximation to the genetic mechanism of scapolite in type-I and type-III samples. The presence of dissolved hydroxides also agrees with the pH range (neutral to moderately alkaline) estimated by DELGADO (1993) for the hydrothermal solutions in the northern skarns of the Maladeta Complex. The values of X and Y, as written in these reactions, are stoichiometric coefficients. If we take into account the relationships between the ratio of the activities of NaCl and $CaCO_3$ in the fluid phase and the composition of the coexisting scapolite derived by ORVILLE (1975) and ELLIS (1978), their ratio (X/Y) is probably proportional to the ratio of the activities of NaCl and $CaCO_3$ in the fluid phase (because the activities are not constrained by stoichiometric criteria). A numerical expression relating X and Y to a_{CaCO3} and a_{NaCl} appears premature, given that no data about the activity-composition relationships in complex $NaCl–H_2O–CO_2$ systems at high temperatures

are available. The proposed reactions schemes (7 and 8) stress the complexity of the fluid phase in these high temperature hydrothermal systems and some of the difficulties that arise in open system environments.

The best examples of plagioclase replacement by scapolite in the studied samples correspond to type-IV rocks (microdiorites). In these samples, textural relationships indicate that primary plagioclase and biotite ($fe^* = 0.43–0.48$; Table 5) are replaced by scapolite and aggregates of titanite and tiny grains of Fe–Ti oxides. Minor amounts of primary Mg-hornblende (Table 4) were probably part of the reaction, but we have excluded them from the reaction for simplicity. As a first constraint to a possible reaction scheme to explain the observed textural relationships, we consider that the composition of the reacting biotite is the main factor that controls the amounts of titanite and opaque minerals (ilmenite) produced by the reaction. Titanite also fixes part of the excess Ca in reactions similar to (7), i.e. when the plagioclase involved in the reaction is more calcic than the resulting scapolite (otherwise, additional Ca would be necessary). As pure biotite end-members (phlogopite, eastonite, annite and siderophyllite) are Ti-free, a biotite composition similar to those analysed in type-IV samples (Table 4), with the general formula $[Si_{2.7}Al_{1.3}]$-$Al_{0.1}Ti_{0.1}Fe_{1.3}Mg_{1.5}K\,O_{10}(OH)_2$ has to be considered. In order to write a generalised reaction scheme, the formula of biotite has been expressed in terms of the formula coefficients $\alpha, \beta, \chi, \delta,$ and ε (each one between the limits imposed by the stoichiometry of this mineral) so the formula of biotite would be expressed as: $Si_\alpha Al_\beta Ti_\chi Fe_\delta Mg_\varepsilon KO_{10}(OH)_2$. The proportions of titanite and ilmenite formed by the reaction were constrained to the same value (each mineral uses half of the available titanium), according to the textural relationships observed in thin section. The proposed reaction scheme is, after simplification of the coefficients and considering the same Si and Al aqueous species as in reactions (7) and (8):

$$A·3An + B·3Ab + D·(Si_\alpha Al_\beta Ti_\chi Fe_\delta Mg_\varepsilon KO_{10}(OH)_2) + X(CO_3Ca)_{fluid} + Y(NaCl)_{fluid} + k(NaOH) + (2k+3D\beta-2D)OH^-$$

$$=$$

$$X·Me + Y·Ma + D·\chi/2(CaTiSiO_5) + D·\chi/2(FeTiO_3) + (k-(D·\chi/2))·Ca^{2+} + (k+D·\beta)(Al(OH)_3)_{aq} + ((D·(\alpha-\chi)-k)SiO_2)_{aq} + D·K^+ + D·Mg^{2+} + D·(\delta-\chi/2)Fe^{2+} + (2·D-2k-3D\beta)·(OH)^- + (D·(10-3\chi-\alpha) + k)O^{2-} \quad (9)$$

This reaction is charge- and mass-balanced for the elements considered. Little is known about the speciation of many elements at high temperature, hence many elements are indicated as ionic components, as suitable species probably involve other elements not considered in the first term of the reaction (Cl^-, S^{2-}, and probably other anions and cations in the fluid phase). The resulting fluid phase is considerably more complex than in the previous case, and other silicates may precipitate from this fluid phase.

The origin of the scapolite vein fillings (Fig. 3) observed in some of the type-III samples may have followed such a scheme. These vein scapolite crystals are commonly associated with calcite and amphibole, and textural relationships indicate direct precipitation rather than replacement of pre-existing mineral phases. These inclusion-free vein-scapolite crystals are in optical and chemical continuity with those in the rocks. Therefore, we suggest that late scapolite was able to grow in veins, directly from a complex fluid phase, that was probably enriched in the excess elements resulting from previous replacement processes.

Conclusions

Scapolite occurs as part of the mineral assemblage of calc-silicate contact metamorphic rocks and microdiorite dykes, over a wide area of the aureole of the Maladeta Plutonic Complex. Crystallographic and compositional (EMP) data presented, together with TGA and IR data, define a calcic (64.7 to 46.7 Me%) composition of all the studied scapolite crystals. Cl-rich compositions (up to 2.35 wt% Cl) were obtained for some of the analysed crystals. The A-site seems to be fully occupied in the analysed scapolite porphyroblasts, Cl and CO_3^{2-} species being the dominant anions (0.43 and 0.49 a.p.f.u., respectively) with SO_3 (0.1 a.p.f.u.) occurring in minor amounts. These data, together with textural relationships of scapolite with plagioclase, in veins, and in recrystallised parts of the studied rocks, support the hypothesis of a common genetic process. This fluid-rock interaction process, was related to a mainly crustal fluid phase rich in CO_3^{2-} and NaCl, as supported by fluid inclusion data for mineralised skarns from the same area. This process postdated the main contact metamorphic event and was probably related to hydrothermal circulation around the Maladeta Complex, which surely increased in response to the thermal gradients set up by the intrusion. Fluid flow was enhanced by the opening of discontinuities in the rocks, mainly microcracks and narrow veins that acted as early conduits for hydrothermal fluids.

Formation of early scapolite poikiloblasts in the studied rocks was probably related to disequilibrium replacement of plagioclase. Taking into account the compositional relationships between coexisting plagioclase and scapolite derived in many studies, the resulting scapolite composition may be related to the composition of the fluid phase by reactions (7) and (8), depending on the composition of scapolite and plagioclase. Inclusion of additional reactants (biotite) and products (titanite, ilmenite) to this scheme, as suggested by textural relationships in type-IV samples, considerably increases the complexity of the reaction scheme and that of the composition of the fluid phase (equation 9).

Later growth of scapolite took place as vein fillings in optical and chemical continuity to those crystals in the adjacent calc-silicate rocks. In this case direct hydrothermal precipitation (rather than replacement) of scapolite, together with other mineral phases (mainly alkali feldspar, amphibole, quartz, calcite, chlorite, and sulfides; pyrrhotite and chalcopyrite) is proposed. The composition of these mineral phases may reflect the composition of the fluid phase resulting from the replacement reactions (equations 7, 8 and 9).

The composition of the involved host rock and fluid phase were the main controlling factors for scapolite growth, as only calc-silicate and microdiorite rocks include scapolite and all of the analysed crystals show a common compositional trend, that is coherent with a post-metamorphic local-scale hydrothermal event around the Maladeta Plutonic Complex.

References

AITKEN, B.G. (1983): T–X_{CO_2} stability relations and phase equilibria of a calcic carbonate scapolite. Geochim. Cosmochim. Acta 47, 351–362.

AITKEN, B.G., EVANS, JR. H.T. and KONNERT, J.A. (1984): The crystal structure of a synthetic meionite. N. Jb. Mineral. Abh. 149, 309–342.

ARRANZ, E. (1997): Petrology of the Maladeta granitic massif (Huesca-Lérida): structure, mineralogy and petrogenesis. (in Spanish). Unpubl. Ph.D. Thesis, University of Zaragoza, Spain. 319 pp.

BARNOLAS, A. and CHIRON, J.C. (1996): Synthèse géologique et géophysique des Pyrénées. Volume 1: Introduction. Géophysique. Cycle hercynien. Edition BRGM-ITGE. 729 pp.

BAYLISS, P. (1987): Mineral nomenclature: scapolite. Mineral. Mag. 51, 176.

BICKLE, M.J., WICKHAM, S.M., CHAPMAN, H.J. and TAYLOR, H.P. JR. (1988): A strontium, neodymium and oxygen isotope study of hydrothermal metamorphism and crustal anatexis in the Trois Seigneurs Massif, Pyrenees, France. Contrib. Mineral. Petrol. 100, 399–417.

BOWERS, T.S. and HELGESON, H.C. (1983a): Calculation of the thermodynamic and geochemical consequences of nonideal mixing in the system H_2O–CO_2–NaCl on phase relations in geologic systems: equation of state for H_2O–CO_2–NaCl fluids at high pressures and temperatures. Geochim. Cosmochim. Acta 47, 1247–1275.

BOWERS, T.S. and HELGESON, H.C. (1983b): Calculation of the thermodynamic and geochemical consequences of nonideal mixing in the system H_2O–CO_2–NaCl on phase relations in geologic systems: metamorphic equilibria at high pressures and temperatures. Am. Mineral. 68, 1059–1075.

BURLEY, J., FREEMAN, E.B. and SHAW, D.M. (1964): Studies on scapolite. Can. Mineral. 19, 670–679.

CRAWFORD, M.L., FILER, J. and WOOD, C. (1979a): Saline fluid inclusions associated with retrograde metamorphism. Bull. Minéralogie 102, 562–568.

CRAWFORD, M.L., KRAUS, D.W. and HOLLISTER, L.S. (1979b): Petrologic and fluid inclusion study of calcsilicate rocks, Prince Rupert, British Columbia. Am. J. Sci. 279, 1135–1159.

CRISS, R.E , FLECK, R.J. and BARNES, I. (1984): Gigantic metamorphic-hydrothermal system around the northern Idaho batholith and its relationship to regional metamorphic zonation. GSA Abstracts with Programs, 16, 479.

CHAMBERLAIN, C.P., DOCKA, J.A., POST, J.E. and BURNHAM, C.W. (1985): Scapolite: alkali atom configurations, antiphase domains, and compositional variations. Am. Mineral. 70, 134–140.

CHARLET, J.M. (1977): Le métamorphisme au contact des granitoïdes entre les vallées de l'Esera et de la Noguera Ribagorzana (Pyrénées centrales espagnoles). Annales de la Société Géologique du Nord, XCVII/3, 165–177.

CHARLET, J.M. (1979): Le Massif Granitique de La Maladeta (Pyrénées Centrales espagnoles). Synthése des données géologiques. Annales de la Société Géologique de Belgique 102, 313–323.

DAWSON, J.B. (1971): Advances in kimberlite geology. Earth-Science Reviews 7, 187–214.

DEBON, F., ENRIQUE, P. and AUTRAN, A. (Coords.)(1996): Magmatisme Hercynien. Chap. 9 In: BARNOLAS, A. and CHIRON, J.C. (eds): Synthèse géologique et géophysique des Pyrénées. Vol. 1, 361–499.

DEER, W.A., HOWIE, R.A. and ZUSSMANN, J. (1963): Rock-forming minerals. Vol. 4. Framework silicates. Longmans, Green and Co., London, 435 pp.

DELGADO, J. (1993): Mineralogical, physical-chemical and geochemical characterization of the northern contact skarns of the Maladeta batholith (Vall d´Aran, Lleida). (in Spanish) Unpubl. Ph.D. Thesis, University of Barcelona, Spain.

ELLIS, D.E. (1978): Stability and phase equilibria of chloride and carbonate bearing scapolites at 750 °C and 4000 bar. Geochim. Cosmochim. Acta 42, 1271–1281.

EVANS, N.G. (1993): Deformation during the emplacement of the Maladeta granodiorite, Spanish Pyrenees. Unpubl. Ph.D. Thesis, University of Leeds.

EVANS, B.W., SHAW, D.M. and HAUGHTON, D.R. (1969): Scapolite stoichiometry. Contrib. Mineral. Petrol. 24, 293–305.

GARCÍA-BELLES, J. (1998): Petrology, structure and geochemistry of dykes and sills in the south margin of the Maladeta Plutonic Complex (Pyrenean Axial Zone; Huesca and Lérida provinces). (in Spanish). Unpubl. M. Sc. Thesis, University of Zaragoza, Spain, 144 pp.

GARCÍA-SANSEGUNDO, J. (1992): Stratigraphy and structure of the Pyrenean Axial Zone through the Valle de Arán and Alta Ribagorça section. (in Spanish). Ph. D. Thesis, University of Oviedo, Spain.

GARVEY, R. (1990): PDFEAPC: a Pc version of NBS*AIDS, A Fortran Program for Crystallographic Data Evaluation by Mighell, A.D; Hubbard, C.R; Stalick, J.K. (1981). NBS Technical Note, 1141.

GLEESON, S.A., WILKINSON, J.J., SHAW, H.F. and HERRINGTON, R.J. (2000): Post-magmatic hydrothermal circulation and the origin of base metal mineralization, Cornwall, UK. J. Geol. Soc. London 157, 589–600.

GOERGEN, E.T., FRUCHEY, B.L. and JOHNSON, E.L. (1999): High Cl amphibole and scapolite from retrograde shear zones in the Dana Hill metagabbro body: evidence of metasomatism within the Carthage-Colton mylonite zone. GSA Abstracts with Programs, 31/7, 168.

GOFF, F.E., ARNEY, B.H. and EDDY, A.C. (1982): Scapolite phenocrysts in a latite dome, northwest Arizona, USA. Earth Planet. Sci. Lett. 60, 86–92.

GOLBERG, J.M., MALUSKI, H. and LEYRELOUP, A.F. (1986): Petrological and age relationship between emplacement of magmatic breccia, alkaline magmatism, and static metamorphism in the North Pyrenean Zone. Tectonophysics 129, 275–290.

GOLBERG, J.M. and LEYRELOUP, A.F. (1990): High temperature-low pressure Cretaceous metamorphism related to crustal thinning (Eastern North Pyrenean Zone, France). Contrib. Mineral. Petrol. 104, 194–207.

GRAZIANI , G. and LUCCHESI, S. (1982): The thermal behavior of scapolites. Am. Mineral. 67, 1229–1241.

HASSAN, I. and BUSECK, P.R. (1988): HRTEM characterization of scapolite solid solutions. Am. Mineral. 73, 119–134.

HUCKENHOLZ, H.G. and SEIBERL, W. (1989): Occurrence of carbonate scapolites and their bearing on geothermometry of (high-temperature) granulite facies. 28th Int. Geol. Congress, Abstracts, Vol. 2, 79–80.

JIANG, S.-Y., PALMER, M.R., XUE, C.-J. and LI, Y-H. (1994): Halogen-rich scapolite-biotite rocks from the Tongmugou Pb-Zn deposit, Qinling, north-western China: implications for the ore-forming processes. Mineral. Mag. 58, 543–552.

KERRICK, D.M., CRAWFORD, K.E. and RANDAZZO, A.F. (1973): Metamorphism of calcareous rocks in three roof pendants in the Sierra Nevada, California. J. Petrol. 14, 303–325.

KULLERUD, K. and ERAMBERT, M. (1999): Cl-scapolite, Cl-amphibole, and plagioclase equilibria in ductile shear zones at Nusfjörd, Lofoten, Norway: Implications for fluid compositional evolution during fluid-mineral interaction in the deep crust. Geochim. Cosmochim. Acta 63/22, 3829–3844.

KWAK, T.A.P. (1977): Scapolite compositional change in a metamorphic gradient and its bearing on the iden-

tification of meta-evaporite sequences. Geol. Mag. 114/5, 343–354.

LAIRD, J. and ALBEE, A.L. (1981): High-pressure metamorphism in mafic schists from Northern Vermont. Am. J. Sci., 281, 97–126.

LIEFTINK, D.J., NIJLAND, T.G. and MAIJER, C. (1993): Cl-rich scapolite from Ødergärdens Verk, Bamble, Norway. Nordsk Geologisk Tidsskrift 73, 55–57.

LOVERING, J.F. and WHITE, A.J.R. (1964): The significance of primary scapolite in granulitic inclusions from deep seated pipes. J. Petrol. 5, 195–218

MARKL, G. and PIAZOLO, S. (1998): Halogen-bearing minerals in syenites and high-grade marbles of Dronning Maud Land, Antarctica: monitors of fluid compositional changes during late-magmatic fluid-rock interaction processes. Contrib. Mineral. Petrol. 132, 246–268.

MEY, P.H.W. (1967a): Evolution of the Pyrenean Basins during the Late Palaeozoic. Proceedings of the First International Symposium on the Devonian System, Calgary, Canada. Canadian Soc. Petrol. Geol. Mem. 2, 1157–1166.

MEY, P.H.W. (1967b): The geology of the Upper Ribagorzana and Baliera Valleys, Central Pyrenees, Spain. Leidse Geologische Mededelingen 41, 153–220.

MOECHER, D.P. and ESSENE, E.J. (1990): Phase equilibria for calcic scapolite and implications of variable Al-Si disorder for P–T, T–X_{CO2}, and a–X relations. J. Petrol. 31/5, 997–1024.

MOINE , B., SAUVAN, P. and JAROUSSE, J. (1981): Geochemistry of evaporite-bearing series: a tentative guide to the identification of metaevaporites. Contrib. Mineral. Petrol. 76, 401–412.

MONTIGNY, R., AZAMBRE, B., ROSSY, M. and THUIZAT, R. (1986): K–Ar study of Cretaceous magmatism and metamorphism in the Pyrenees: age and length of rotation of the Iberian Peninsula. Tectonophysics 129, 257–273.

MORA, C.I. and VALLEY, J.W. (1989): Halogen-rich scapolite and biotite: implications for metamorphic fluid-rock interaction. Am. Mineral. 74, 721–737.

OLIVER, N.H.S., WALL, V.J. and CARTWRIGHT, I. (1992): Internal control of fluid compositions in amphibolite-facies scapolitic calc-silicates, Mary Kathleen, Australia. Contrib. Mineral. Petrol. 111, 94–112.

ORVILLE, P.M. (1975): Stability of scapolite in the system Ab–An–NaCl–$CaCO_3$ at 4 kbar and 750 °C. Geochim. Cosmochim. Acta 39, 1091–1105.

OTERDOOM, W.H. and GUNTER, W.D. (1983): Activity models for plagioclase and CO3 scapolites – an analysis of field and laboratory data. Am. J. Sci., V. 283-A, 255–282.

OWEN, J.V. and GREENOUGH, J.D. (1999): Scapolite pegmatite from the Minas fault, Nova Scotia: tangible manifestation of Carboniferous, evaporite derived hydrothermal fluids in the western Cobequid highlands? Mineral. Mag. 63/3, 387–397.

PAN, Y., FLEET, M.E. and RAY, G.E. (1994): Scapolite in two Canadian gold deposits: Nickel Plate, British Columbia and Hemlo, Ontario. Can. Mineral. 32, 825–837.

POBLET, J. (1991): Hercynian and alpine structure of the southern-central Pyrenean axial zone. (in Catalan). Unpubl. Ph.D. Thesis. University of Barcelona, Spain. 604 pp.

RAVIER, J. (1959): Le métamorphisme des terrains secondaires des Pyrénées. Mem. Soc. Geol. France, XXXVIII /86, 250 pp.

RAVIER, J. and THIEBAUT, J. (1982): Sur l'origine lagunaires des marbres et cornéenne mésozoiques du col d'Agnes (Ariège). C.R. Acad. Sci. París, Sér. II, 294, 127–130.

REBBERT, C.R. and RICE, J.M. (1997): Scapolite-plagioclase exchange: Cl–CO_3 scapolite solution chemistry and implications for peristerite plagioclase. Geochim. Cosmochim. Acta. 61/3, 555–567.

REED, S.J.B. (1993): Electron Microprobe Analysis. Cambridge University Press, 2nd Ed., 326 pp.

SCHWARCZ, H.P. and SPEELMAN, E.L. (1965): Determination of sulfur and carbon coordination in scapolite by infra-red absorption spectrophotometry. Am. Mineral. 50, 656–666.

SHAW, D.M. (1960a): The geochemistry of scapolite. Part I. Previous work and general mineralogy. J. Petrol. 1, 218–260.

SHAW, D.M. (1960b): The geochemistry of scapolite. Part II. Trace elements, petrology and general geochemistry. J. Petrol. 1, 261–285.

SOLÉ, J., SOLER, A., PALAU, J., ESPINOLA, M.R. and DELGADO, J. (1997): K/Ar geochronology of the As–Au mineralized skarns and associated intragranitic alterations in the Hercynian of the Central Pyrenees. (in Spanish). Boletin Sociedad Española Mineralogía, 20-A, 77–78.

STOLZ, A. (1987): Fluid activity in the lower crust and upper mantle: mineralogical evidence bearing on the origin of amphibole and scapolite in ultramafic and mafic granulite xenoliths. Mineral. Mag. 51, 719–732.

SWAYZE, G.A. and CLARK, R.N. (1990): Infrared spectra and crystal chemistry of scapolites: implications for Martian mineralogy. J. Geophys. Res. 95, 14481–14495.

TEERSTRA, D.K. and SHERRIFF, B.L. (1996): Scapolite cell-parameter trends along the solid-solution series. Am. Mineral. 81, 169–180.

TEERSTRA, D.K. and SHERRIFF, B.L. (1997): Substitutional mechanisms, compositional trends and the end-member formulae of scapolite. Chem. Geol. 136, 233–260.

TEERSTRA, D.K., SCHINDLER, M., SHERRIFF, B.L. and HAWTHORNE, F.C. (1999): Silvialite, a new sulfate-dominant member of the scapolite group with an Al-Si composition near the I4/m-P4$_2$/n phase transition. Mineral. Mag. 63/3, 321–329.

VANKO, D.A. and BISHOP, F.C. (1982): Occurrence and origin of marialitic scapolite in the Humboldt Lopolith, N.W. Nevada. Contrib. Mineral. Petrol. 81, 277–289.

WHITE, A.J.R. (1959): Scapolite-bearing marbles and calc-silicate rocks from Tungkillo and Milendella, South Australia. Geol. Mag. 96, 285–306.

WICKHAM, S.M. and OXBURGH, E.R. (1986): A rifted tectonic setting for Hercynian high thermal gradient metamorphism in the Pyrenees. Tectonophysics 129, 53–69.

WICKHAM, S.M. and TAYLOR, H.P. (1987): Stable isotope constraints on the origin and depth of penetration of hydrothermal fluids associated with Hercynian regional metamorphism and crustal anatexis in the Pyrenees. Contrib. Mineral. Petrol. 95, 255–268.